Uncertainty Analysis of Multifunctional Constitutive Relations and Adaptive Structures

Paul Miles

Department of Mechanical Engineering
Florida Center for Advanced Aero-Propulsion (FCAAP)
Florida A & M and Florida State University, Tallahassee, FL 32310

Outline

- Background and Motivation
- Uncertainty Quantification
- Dielectric Elastomers
  - Viscoelasticity
  - Electrostriction
- Ferroelectrics
  - Quantum informed continuum modeling
- Future Work

Background & Motivation

- Quantity of Interest
  - Experimental measurements
  - Derive theoretical models
  - Perform numerical simulations
- Uncertainty
  - Measurement error
  - Modeling assumptions
  - Numerical methods

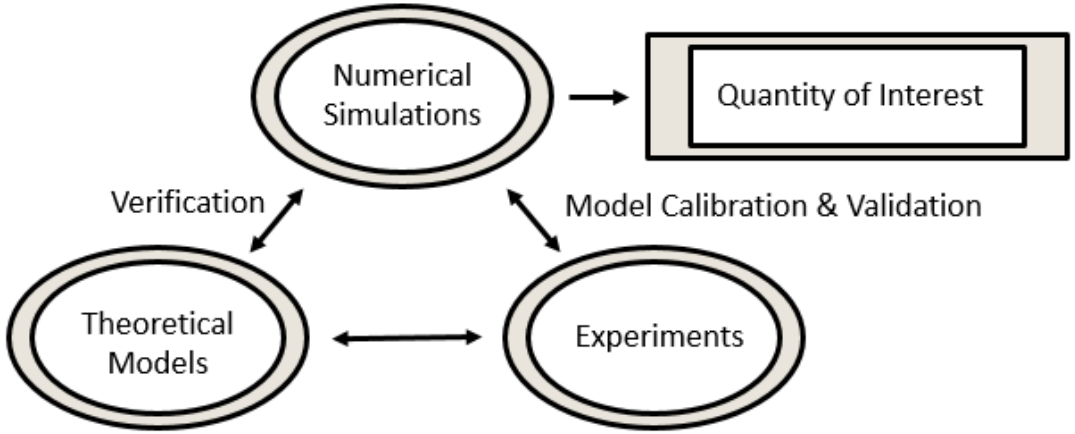

Figure: Components of predictive science: modeling, numerical, and experimental research. Each component contains different aspects of uncertainty[1].

1. Smith, R.. Uncertainty quantification: theory, implementation, and applications, volume 12. SIAM, 2013.

Background & Motivation

- Uncertainty quantification has been applied to a wide variety of disciplines:
  - Atomistic potentials[1], computational fluid dynamics[2], weather prediction[3]
  - Less work has been done in quantifying uncertainty of material models
- Challenges
  - Uncertainty propagates across scales - atomic structures to continuous media
  - Multiple sources of evidence

1. Frederiksen, S., et al. "Bayesian Ensemble Approach to Error Estimation of Interatomic Potentials." Physical review letters 93.16 (2004): 165501.
2. Croicu, A., et al. "Robust Airfoil Optimization Using Maximum Expected Value and Expected Maximum Value Approaches." AIAA journal 50.9 (2012): 1905-1919.
3. Wilks, D. Statistical Methods in the Atmospheric Sciences. Vol. 100. Academic press, 2011.

Uncertainty Quantification

Uncertainty Quantification: Bayesian Statistical Analysis

- Statistical Model: $M^{data}(i) = M(i;\theta) + \varepsilon_i, \quad i = 1, \ldots, N$
- Bayes' Relation

$$\pi\left(\theta \middle| M^{data}\right) = \frac{p(M|\theta)\pi_0(\theta)}{\int_{\mathbb{R}_p} p(M|\theta)\,\pi_0(\theta)d\theta}$$

- Posterior Density: $\pi\left(\theta \middle| M^{data}\right)$
- Prior Density: $\pi_0(\theta)$
- Likelihood Function: $p(M|\theta) = e^{-\sum_{i=1}^{n}\left[M^{data}(i)-M(i;\theta)\right]^2/(2\sigma^2)}$
  - Assume observation errors are independent and identically distributed (iid): $\varepsilon_i \sim N(0, \sigma^2)$.

Uncertainty Quantification: Bayesian Statistical Analysis

- Markov Chain Monte Carlo (MCMC)
  - Random sampling
- Delayed Rejection Adaptive Metropolis (DRAM)[1,2]
  - Accept proposal based on probability

$$\alpha = \min(1, \frac{p(M|\theta_{new})}{p(M|\theta_{old})})$$

1. Heikki Haario, Marko Laine, Antonietta Mira, and Eero Saksman. DRAM: Efficient Adaptive MCMC. Statistics and Computing, 16(4):339–354, 2006.
2. Heikki Haario, Eero Saksman, and Johanna Tamminen. An Adaptive Metropolis Algorithm. Bernoulli, pages 223–242, 2001.

Uncertainty Quantification: Bayesian Statistical Analysis

- Uncertainty Propagation: Prediction and Credible Intervals

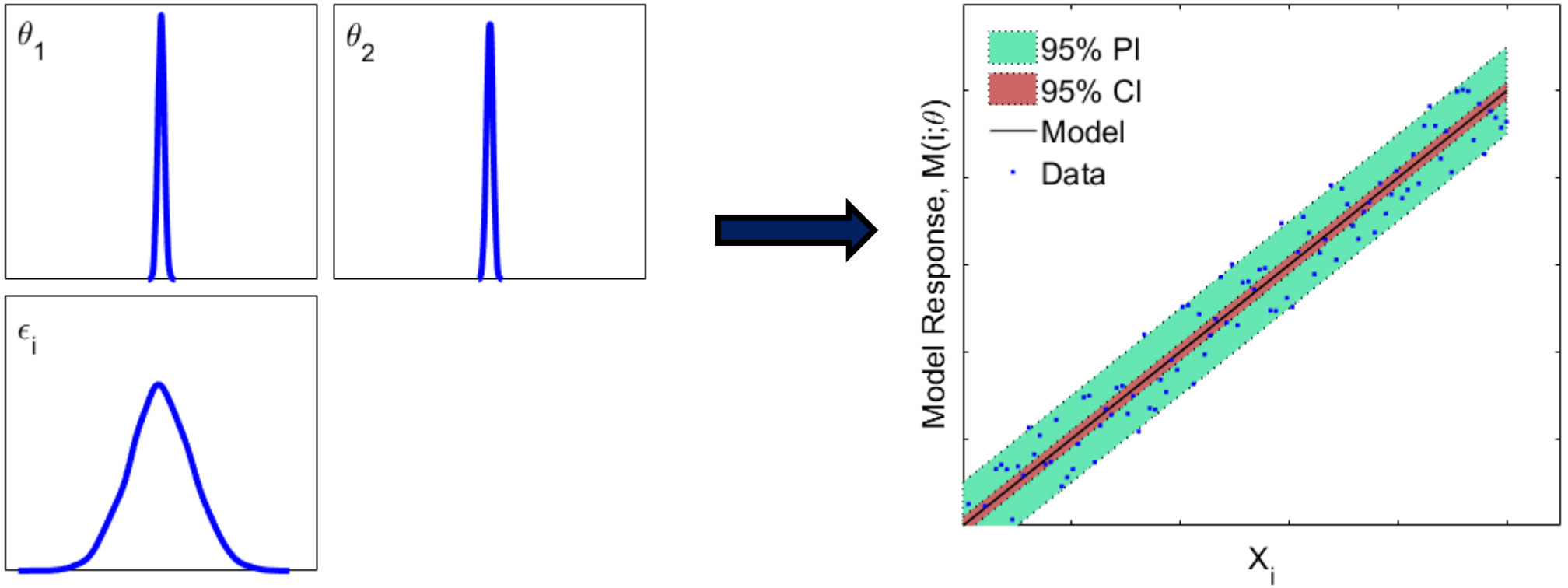

Dielectric Elastomers: Viscoelasticity

Dielectric Elastomers

- Applications:
  - Robotics
  - Flow control
  - Energy harvesting
  - Optical switches

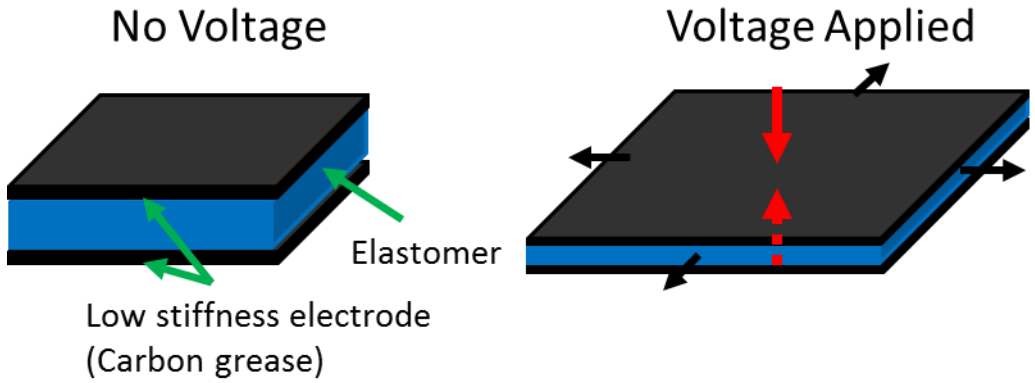

Figure: Out of plane expansion of elastomer as a result of transverse field.

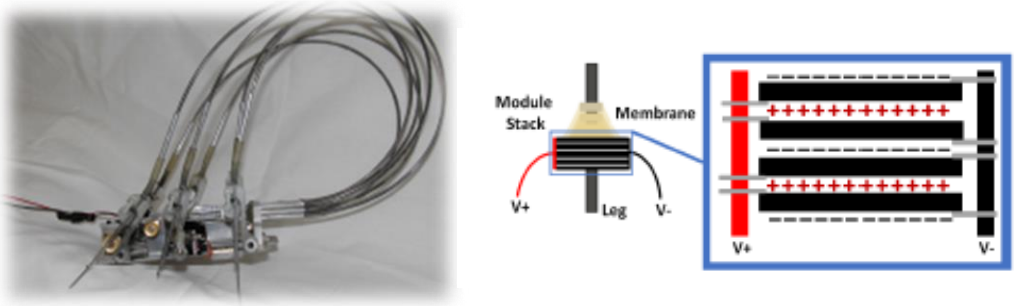

Figure: iSprawl robotic platform[1]. Membrane actuators control leg stiffness allowing for dynamic adaptation to different terrains.

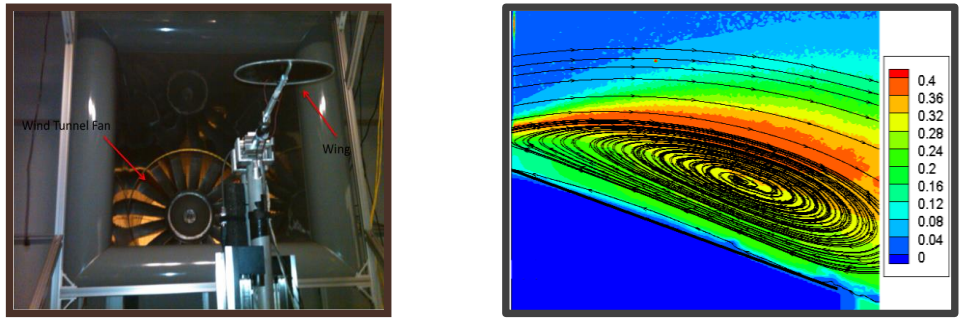

Figure: Wind tunnel experiments with deformable dielectric membrane[2]. By adjusting the membrane stiffness, the wing profile subsequently changed its shape and altered the flow characteristics.

1. Newton, J., "Design and Characterization of a Dielectric Elastomer Based Variable Stiffness Mechanism for Implementation onto a Dynamic Running Robot," (2014), Figure 2.11 and Figure 4.5.
2. Hays, et al. "Aerodynamic Control of Micro Air Vehicle Wings Using Electroactive Membranes," J. Mater. Syst. Struct., v. 24(7), pp. 862-878, 2013.

Dielectric Elastomers: Viscoelasticity - Outline

- Experimental Setup and Observations
- Theory
- Uncertainty Quantification
- Conclusions and Future Work

Experimental Setup

- Very High Bond (VHB) 4910
- Specimens cycled
- Stretch rate: $\frac{\mathrm{d}\lambda}{dt} = \frac{1}{L_0}\frac{dx}{dt}$
  - $\frac{d\lambda}{dt}$ is the stretch rate (Hz)
  - $\frac{dx}{dt}$ is the speed of the moving clamp head (mm/s)
  - L_0 is the initial length of the VHB specimen (mm)

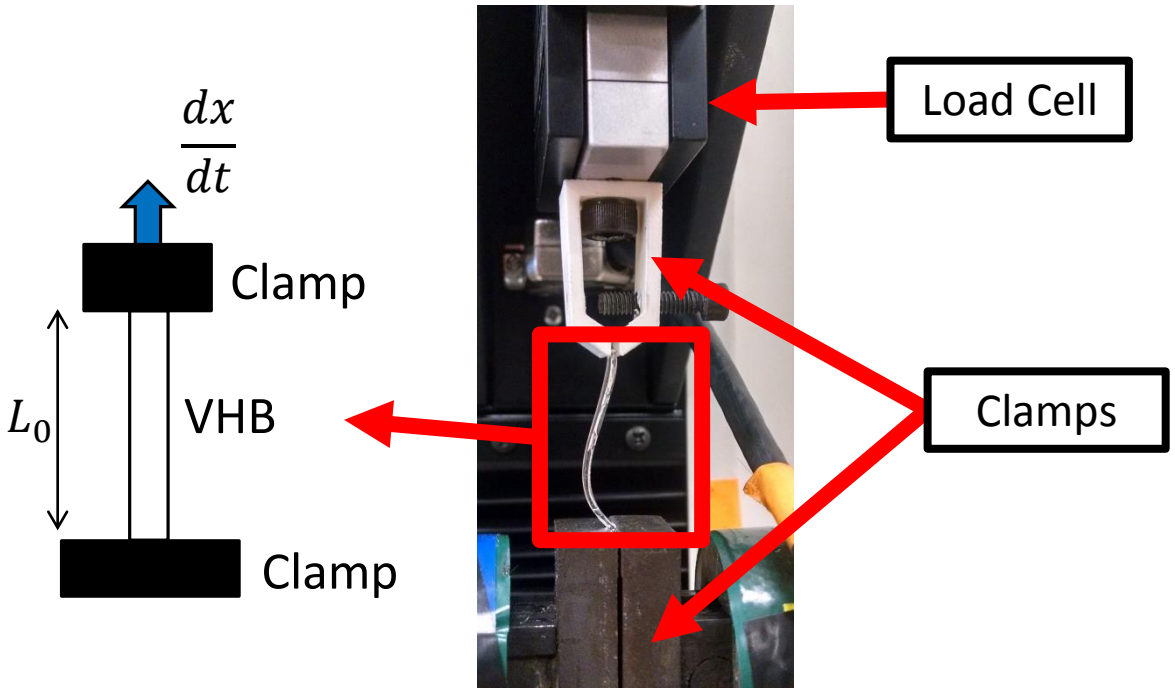

Figure: MTS tensile testing of VHB 4910

Experimental Observations

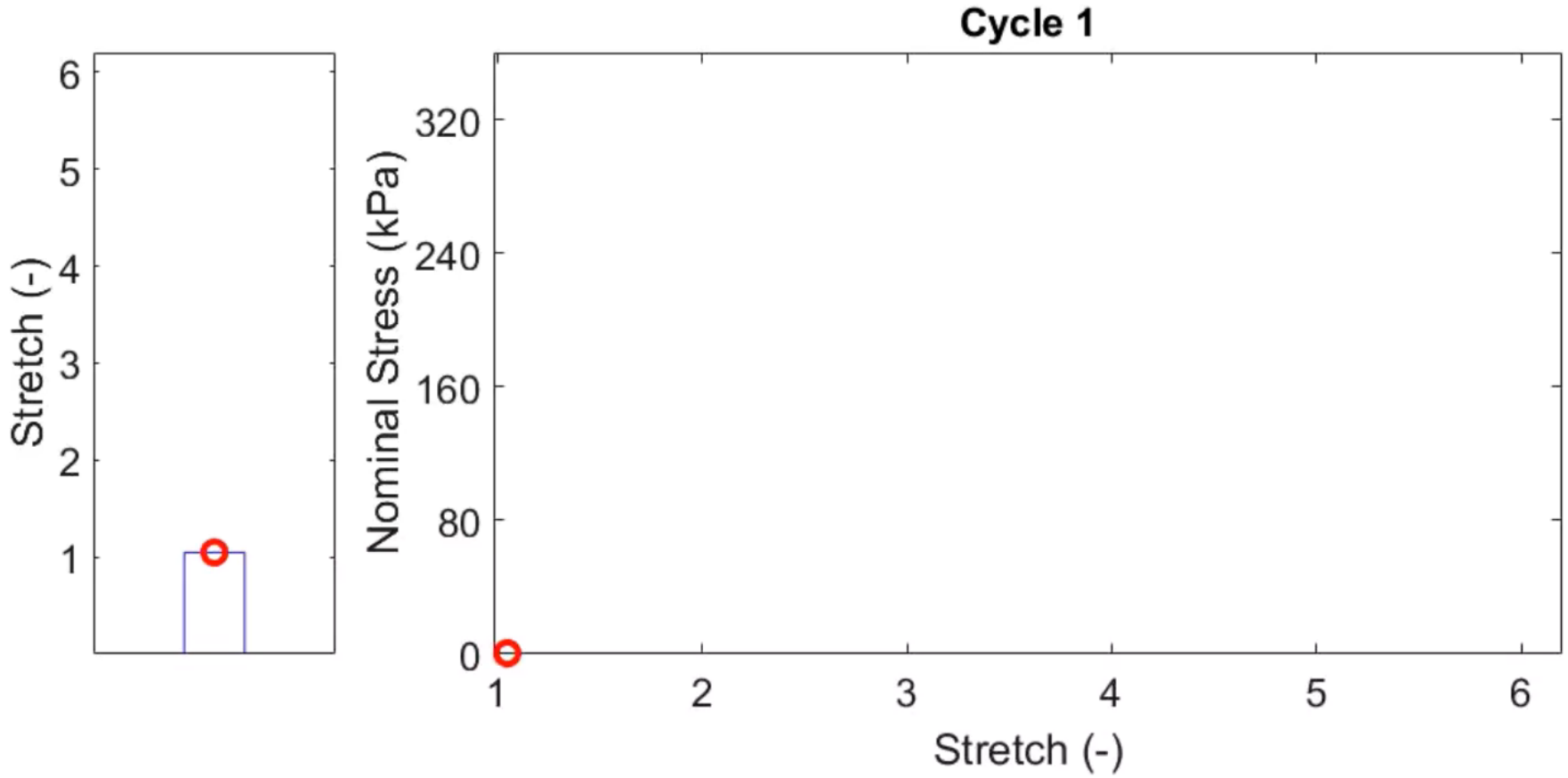

Experimental Observations

- Hysteresis
- Stress response decays
- Recovery
- Steady state

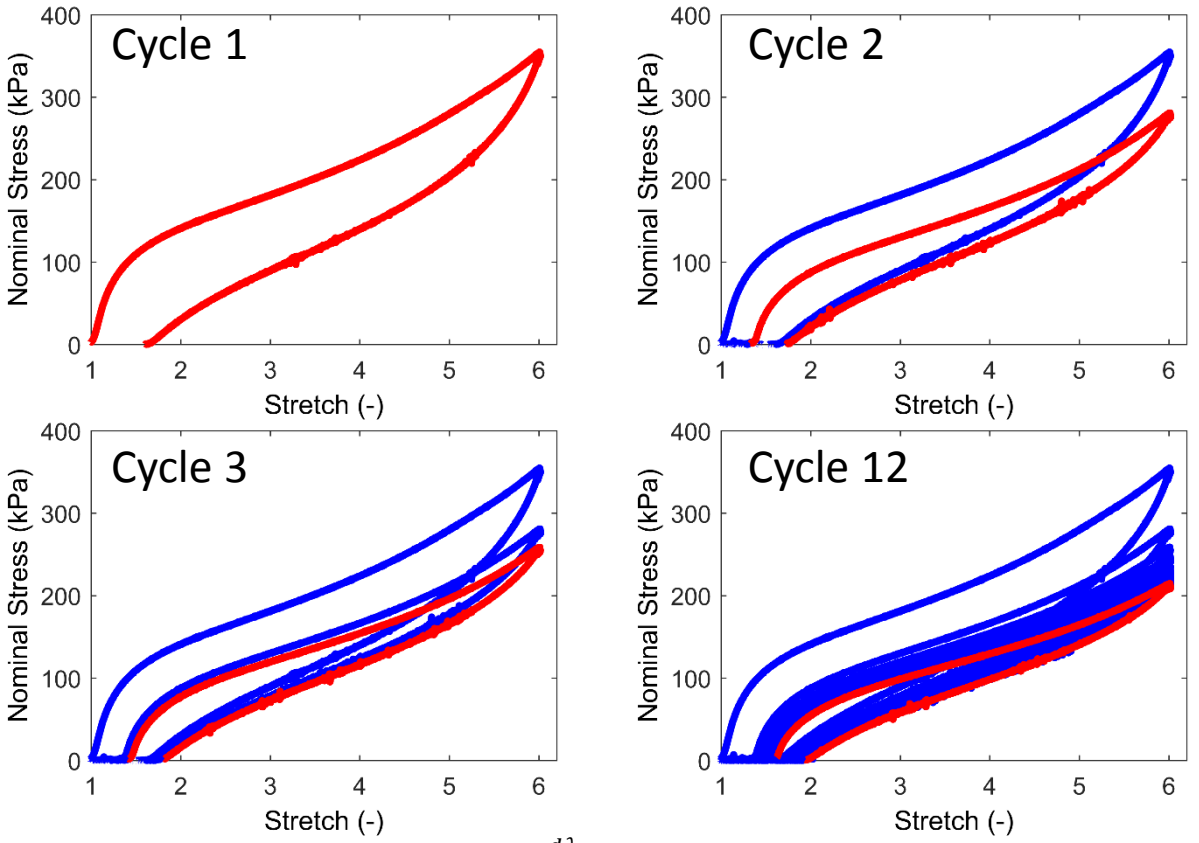

Figure: Cyclic loading of VHB 4910 at $\frac{d\lambda}{dt} = 0.67\ Hz$. Steady state hysteresis observed by the 12th cycle.

Experimental Observations

- Steady state hysteresis
- Rate-dependence
- Uncertainty
  - Measurement
  - Specimen variability

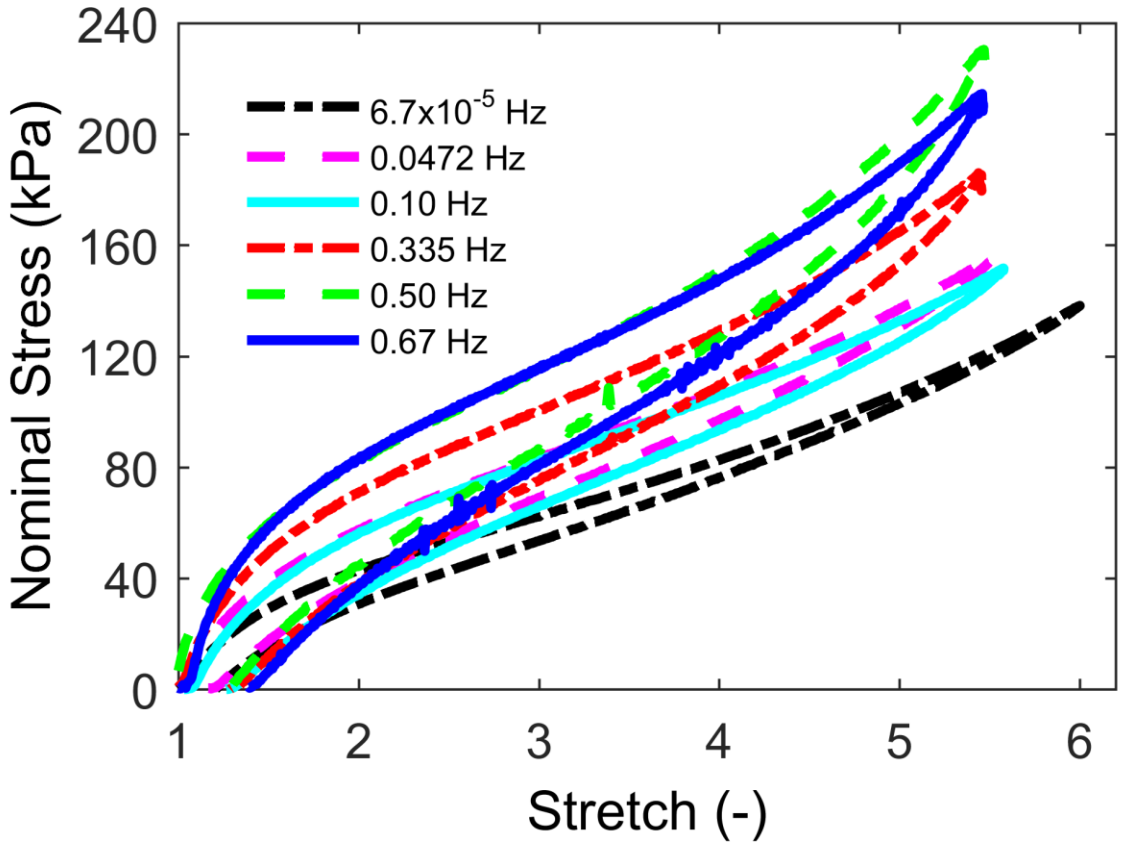

Figure: Steady state hysteresis loops from all stretch rates tested.

Theory: Viscoelasticity

- Total Energy Density

$$\psi = \psi_\infty(F_{iK}, \Theta) + \Upsilon(F_{iK}, \Theta, \Gamma^\nu_{iK})$$

- Nominal Stress

$$s_{iK} = \frac{\partial \hat{\psi}}{\partial F_{iK}} = \frac{\partial \psi_\infty}{\partial F_{iK}} - pJH_{iK} + \frac{\partial \Upsilon}{\partial F_{iK}}$$

- Viscoelastic Stress

$$Q^\nu_{iK} = -\frac{\partial \hat{\psi}}{\partial \Gamma^\nu_{iK}} = -\frac{\partial \Upsilon}{\partial \Gamma^\nu_{iK}}$$

- Components
  - ψ_∞ - conserved, hyperelastic energy function
  - Υ - energy function that depends on non-conserved internal state
  - F_{iK} - deformation gradient
  - Θ - temperature
  - Γ^ν_{iK} - set of non-conserved internal strains

Theory: Viscoelasticity

- Conserved, hyperelastic energy function[1]

$$\psi_\infty = \frac{1}{6} G_c I_1 - G_c \lambda_{max}^2 \log(3\lambda_{max}^2 - I_1) + G_e \sum_j (\lambda_j + \frac{1}{\lambda_j})$$

- Non-conserved energy functions: Linear and Non-linear[2]

$$\Upsilon_L = \sum_\nu [\frac{1}{2} \gamma_\nu (F_{iK} - \Gamma_{iK}^\nu)(F_{iK} - \Gamma_{iK}^\nu)]$$

$$\Upsilon_{NL} = \sum_\nu [\frac{1}{2} \gamma_\nu \Gamma_{iK}^\nu \Gamma_{iK}^\nu - \beta_\infty^\nu \frac{\partial \psi_\infty}{\partial F_{iK}} \Gamma_{iK}^\nu + \beta_\infty^\nu \psi_\infty]$$

- Components
  - G_c - Crosslink modulus
  - G_e - Entanglement modulus
  - λ_{max} - Maximum extension of affine tube
  - β_∞^ν - Phenomenological set of parameters
  - γ_ν - Proportional to viscosity of polymer network

1. Davidson, Jacob D., and N. C. Goulbourne. "A nonaffine network model for elastomers undergoing finite deformations." Journal of the Mechanics and Physics of Solids 61.8 (2013): 1784-1797.
2. Holzapfel & Simo, Int. J. Solid Struct., (1996), v. 33(20-22), pp. 3019-3034.

Parameter Estimation: Viscoelasticity

- Calibrated with data:

$$\frac{d\lambda}{dt} = 6.5 \times 10^{-5}\ Hz$$

- Parameter chains
- Posterior densities

$$\pi\left(\theta \middle| M^{data}\right)$$

- Convergence:
  - "Burned-In"

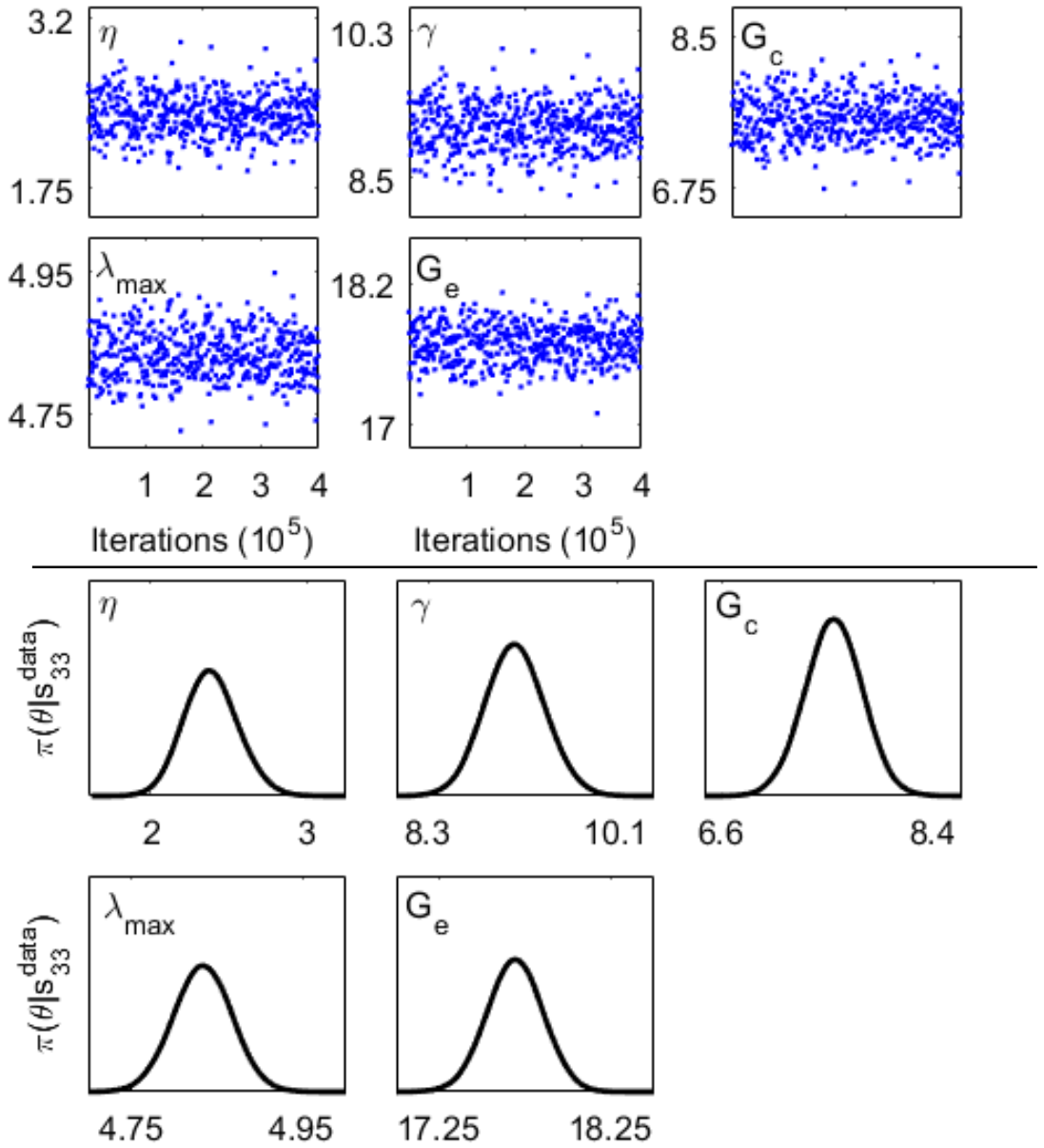

Parameter Correlation: Viscoelasticity

- Pairwise correlation
- Nearly single valued
- Sensitivity

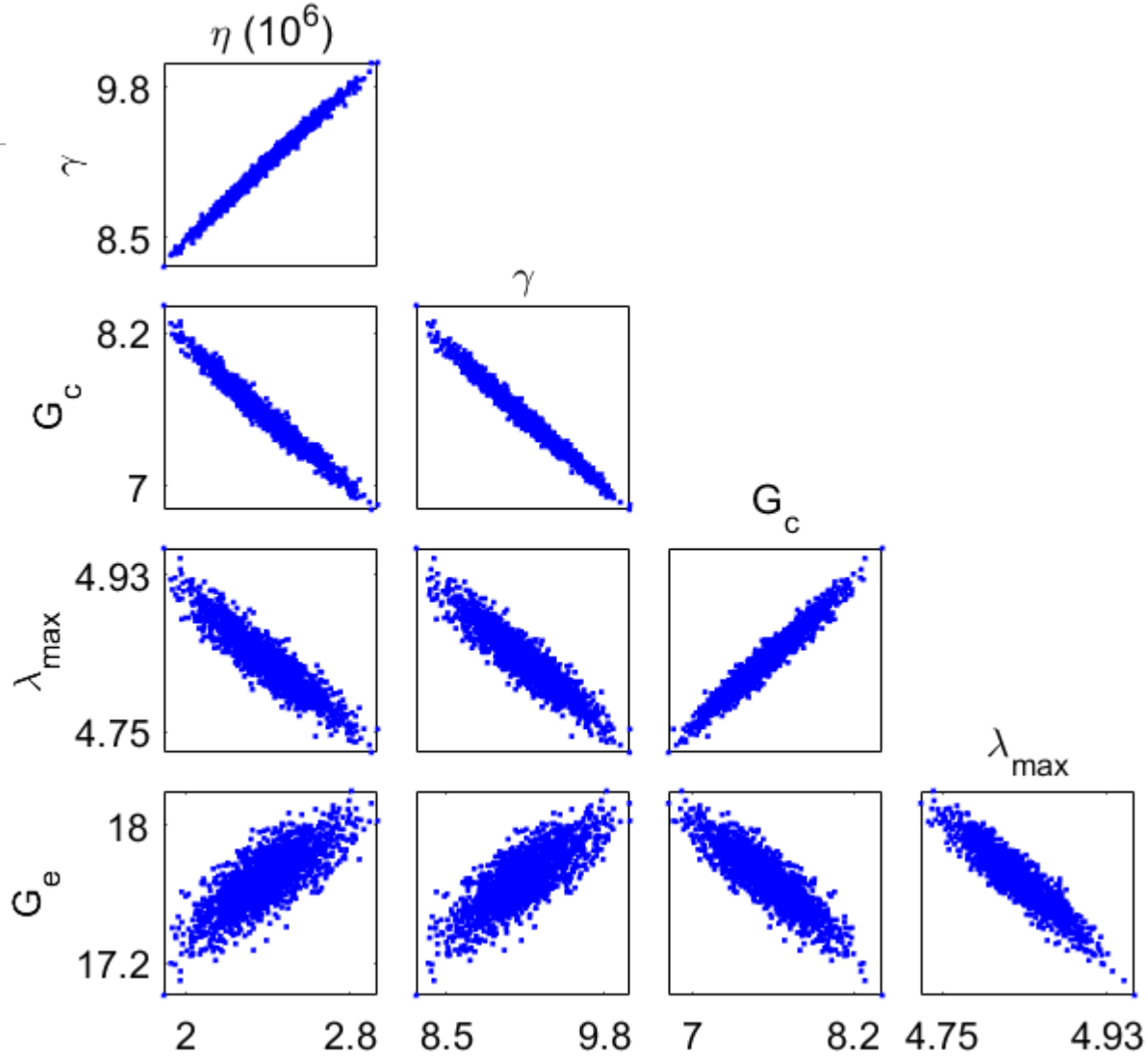

Uncertainty Propagation: Viscoelasticity

- Linear viscoelasticity
- Calibrated at each rate separately

Calibrated Rate (1/s)	$\bar{\eta}$ (kPa·s)	$\bar{\gamma}$ (kPa)
6.7×10^{-5}	2.38×10^{6}	9.12
0.0472	7.36×10^{3}	17.3
0.335	1.84×10^{2}	32.6
0.67	7.37×10^{2}	33.4

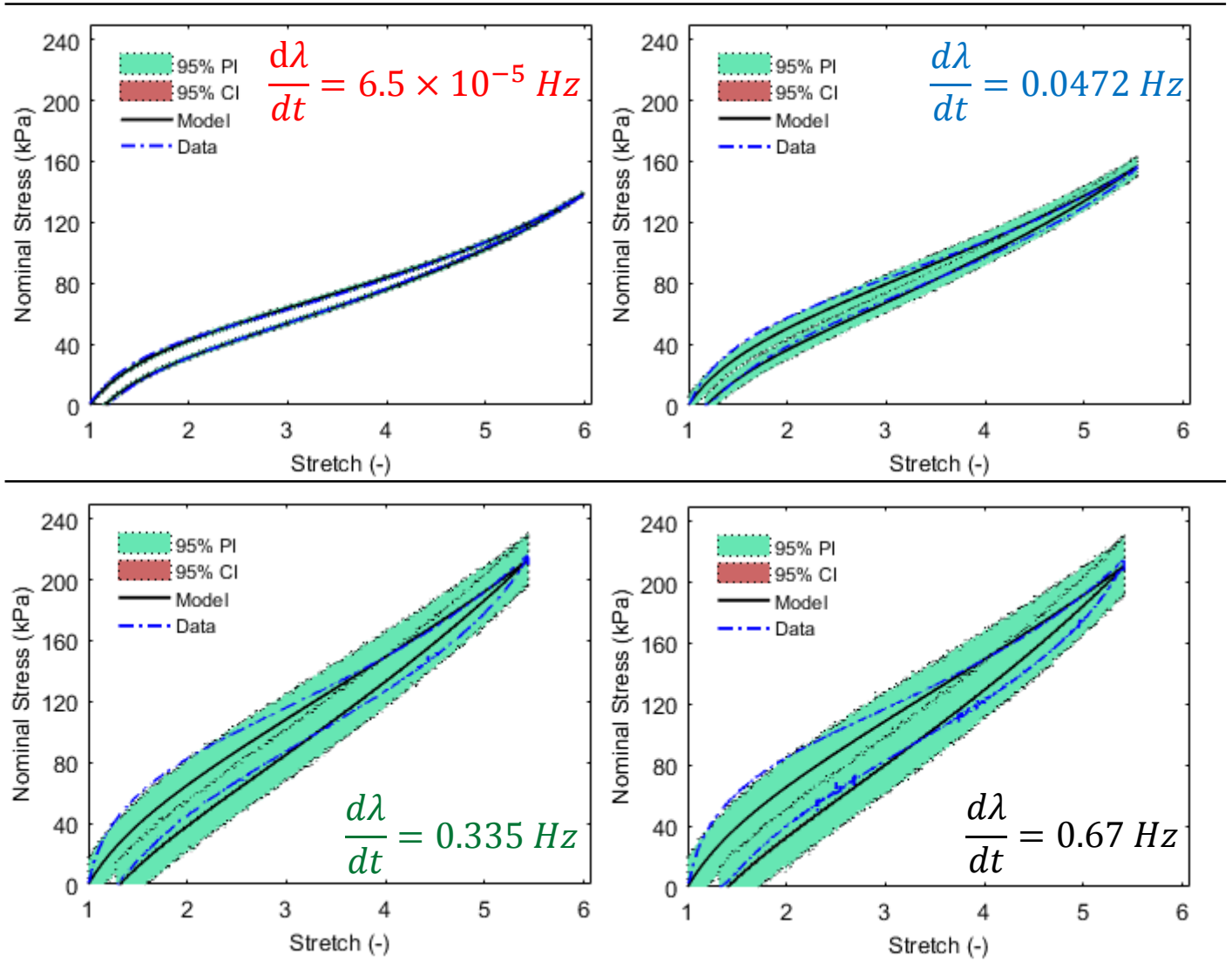

Uncertainty Propagation: Viscoelasticity

- C – Calibrated
- P – Predicted

- Linear viscoelasticity
- First order rate model

$$Q_{iK} = \eta \frac{d\Gamma_{iK}}{dt}$$

Calibrated Rate (1/s)	$\bar{\eta}$ (kPa·s)	$\bar{\gamma}$ (kPa)
6.7×10^{-5}	2.38×10^{6}	9.12

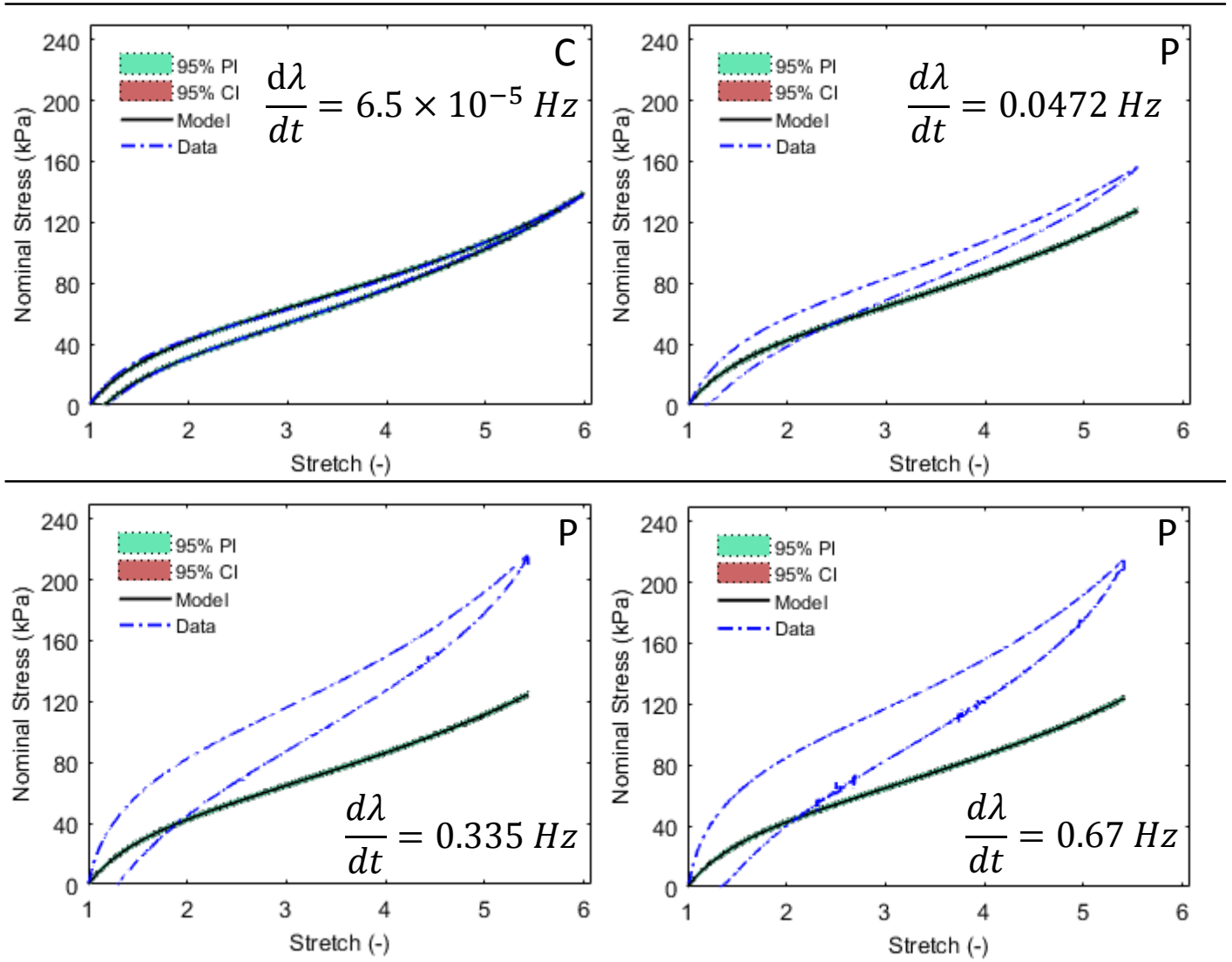

Theory: Viscoelasticity

- Integer order
  - Model limitation
  - Parameters are rate dependent
- Fractional order[1]
  - Replace standard calculus operators with fractional order operators

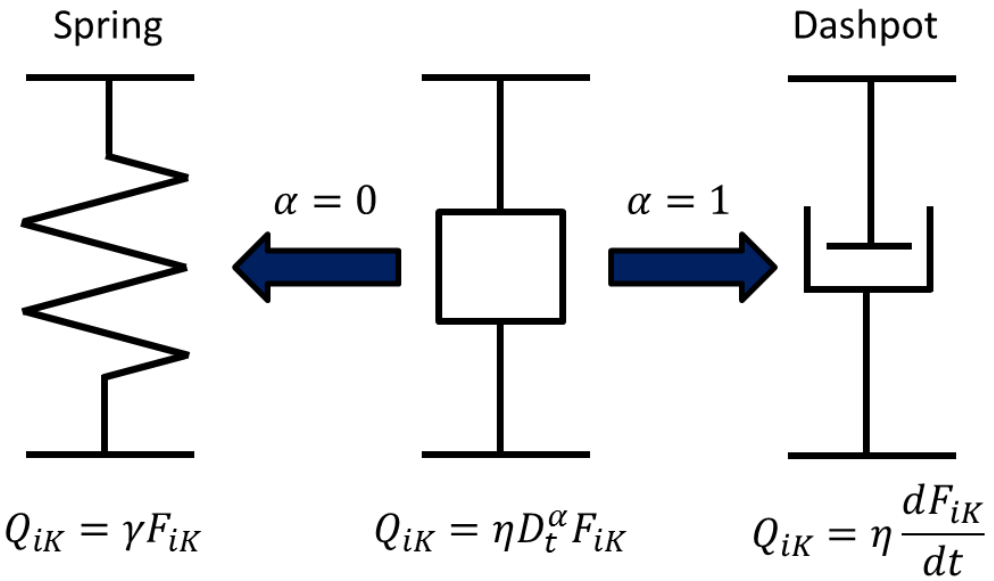

Figure: Fractional order spring-dashpot system. As the fractional order approaches 0 the system behaves like a dashpot. Likewise, as the fractional order approaches 1 the system behaves like a spring.

$$D^{\alpha} f(t) = \frac{1}{\Gamma(n-\alpha)} \int_0^t \frac{f^n(s)}{(t-s)^{\alpha+1-n}} ds, \qquad n-1 < \alpha \leq n, \qquad n \in \mathbb{N}$$

1. Special thanks to Dr. Somayeh Mashayekhi and her assistance in implementing fractional order methods.

Uncertainty Propagation: Viscoelasticity

- C – Calibrated
- P – Predicted

- Linear viscoelasticity
- Fractional order rate relation

$$Q_{iK} = \eta D_t^{\alpha} F_{iK}$$

Calibrated Rate (1/s)	$\bar{\eta}$ (kPa·s)	$\bar{\alpha}$ (-)
6.7×10^{-5}	35.3	0.12

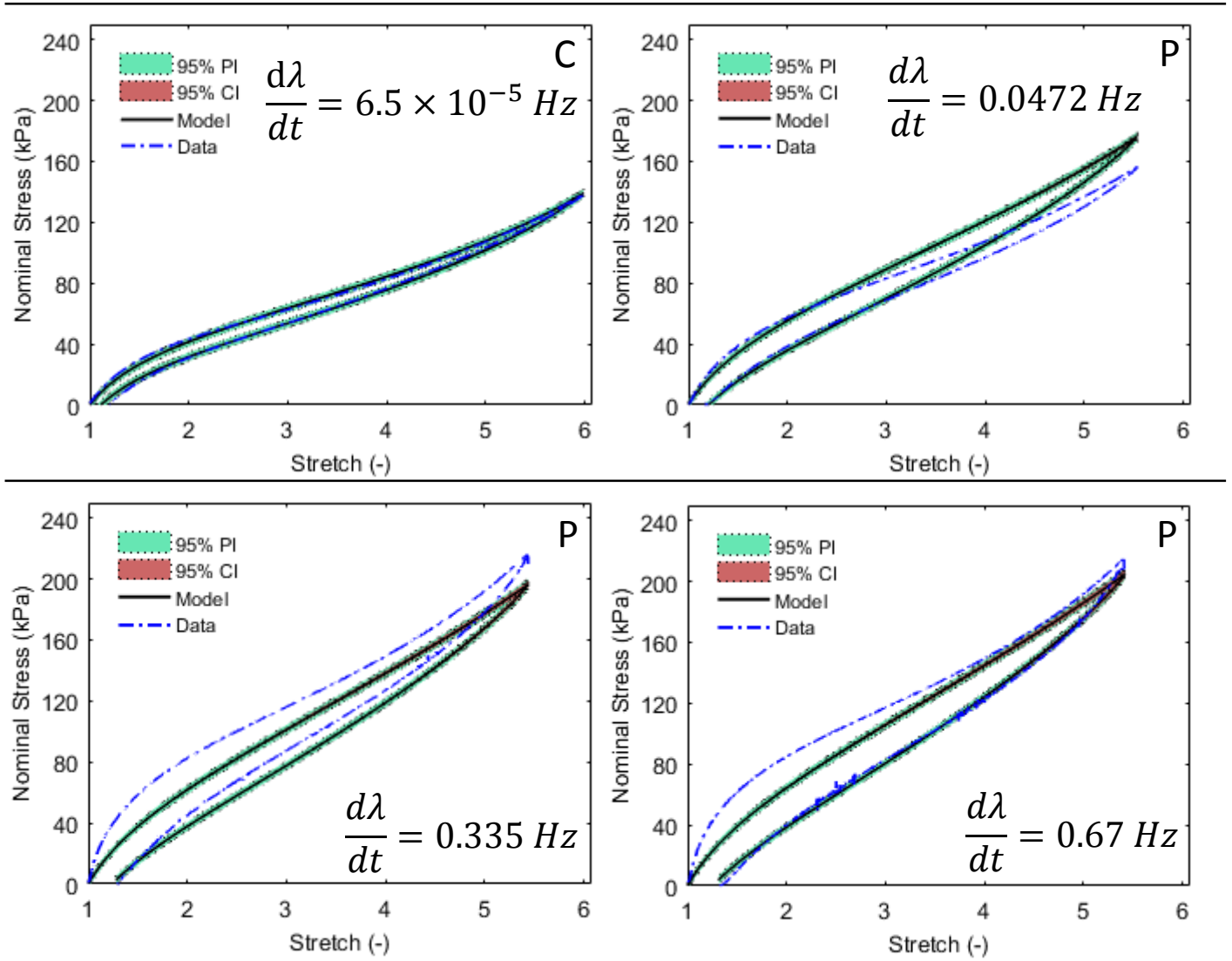

Uncertainty Propagation: Viscoelasticity

- C – Calibrated
- P – Predicted

- Non-linear viscoelasticity
- Fractional order rate relation

$$Q_{iK} = \eta D_t^{\alpha} s_{iK}^{\infty}$$

Calibrated Rate (1/s)	$\overline{\eta}$ (kPa·s)	$\overline{\gamma}$ (kPa)	$\overline{\beta}$ (-)	$\overline{\alpha}$ (-)
0.67	2.32	14.0	0.89	0.17

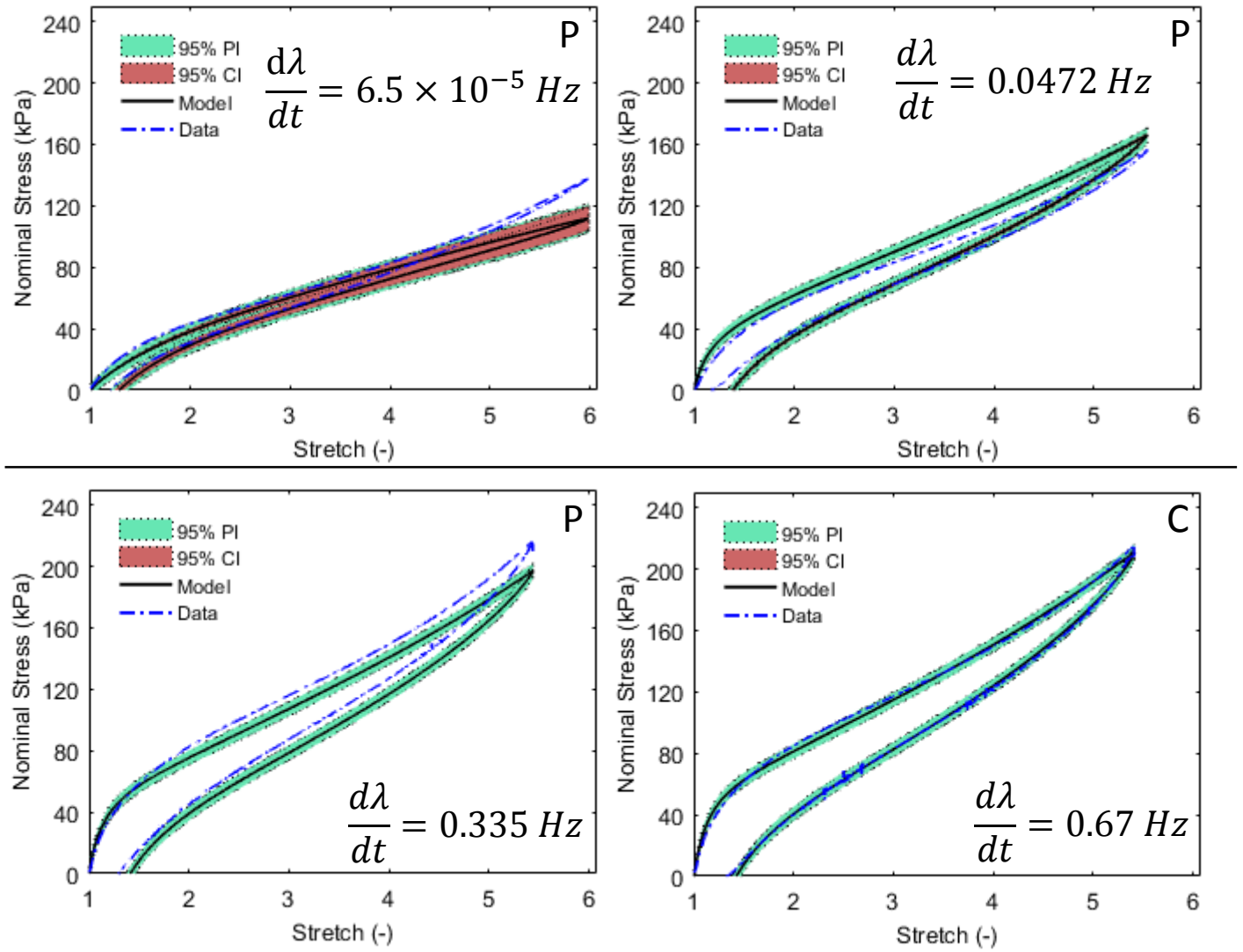

Conclusions & Future Work: Viscoelasticity

- Integer order
  - Parameters are rate-dependent
- Fractional order
  - Predicts behavior over broad range of operating regimes
  - Parameters are independent of rate
- Linear and non-linear
  - Non-linear model improves accuracy, but increases computational cost

Publications: Viscoelasticity

Publications:

- Oates, W., Miles, P., Gao, W., Clark, J., Mashayekhi, S., Hussaini, M.Y. "**Rate Dependent Constitutive Behavior of Dielectric Elastomers and Applications in Legged Robotics**." *SPIE Smart Structures and Materials + Nondestructive Evaluation and Health Monitoring*, 2017.
- Miles, P., Hays, M., Smith, R., Oates, W. "**Bayesian Uncertainty Analysis of Finite Deformation Viscoelasticity**." *Mechanics of Materials*, 2015, Vol. 91, pp. 35-49.
- Miles, P., Hays, M., Smith, R., Oates, W. "**Uncertainty Analysis of a Finite Deformation Viscoelastic Model**." *ASME Smart Materials, Adaptive Structures, and Intelligent Systems*, 2014.
- Oates, W., Hays, M., Miles, P., Smith, R. "**Uncertainty Quantification and Stochastic Based Viscoelastic Modeling of Finite Deformation Elastomers**." *SPIE Smart Structures and Materials + Nondestructive Evaluation and Health Monitoring*, 2013.

Pending Publications:

- Mashayekhi, S., Miles, P., Hussaini, M. Y., Oates, W. "**Fractional Viscoelasticity in Fractal and Non-Fractal Media: Theory, Experimental Validation, and Uncertainty Analysis**." *Mechanics and Physics of Solids*, 2017, submitted for review.

Dielectric Elastomers: Electrostriction

Dielectric Elastomers: Electrostriction - Outline

- Experimental Observations
  - Transverse load – displacement
  - Electric displacement – electric field
- Theory
- Uncertainty Quantification
- Conclusions and Future Work

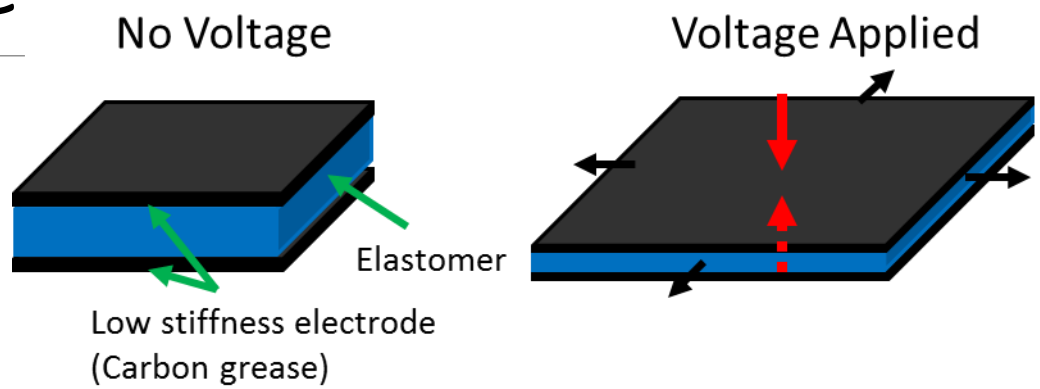

Figure: Out of plane expansion of elastomer as a result of transverse field.

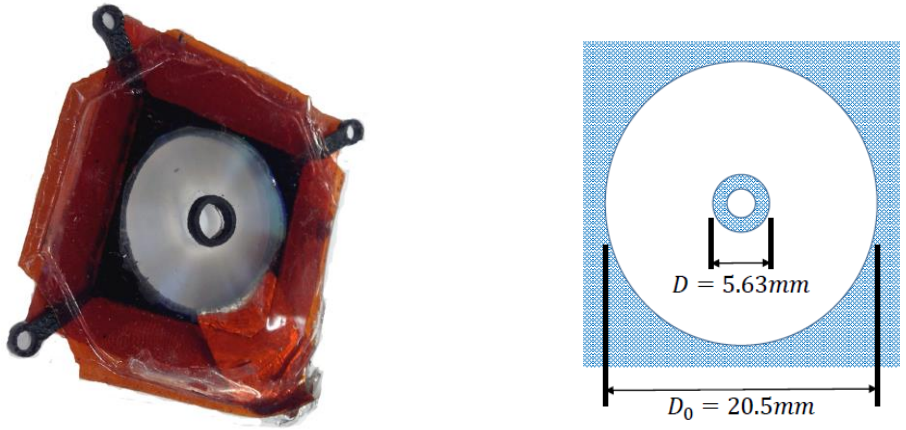

Figure: (Left) Elastomer is stretched over acrylonitrile butadiene styrene (ABS) plastic frame and electrically isolated for electrode application. (Right) Top view of experimental setup.

Experimental Setup: Transverse Force – Displacement

- Very High Bond (VHB) 4910
- Triangular load/unload cycle
- Test cases: $0 - 6\ kV$

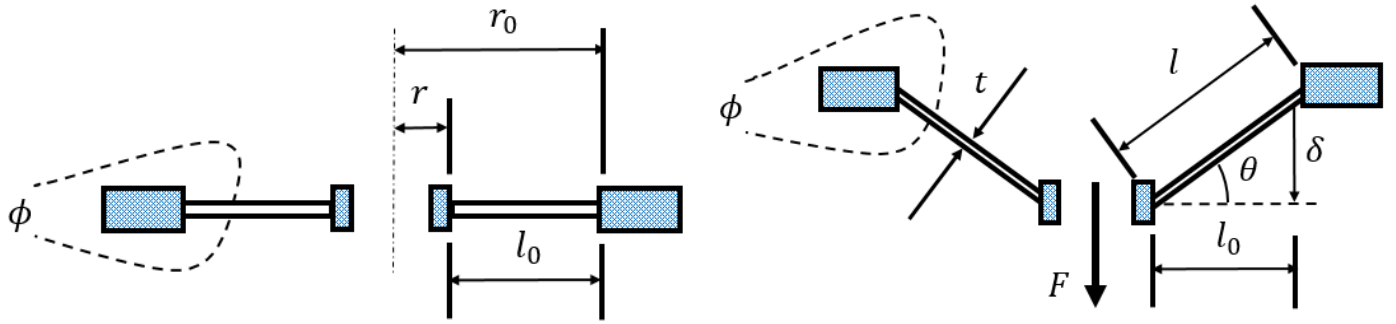

Figure: Schematic of problem geometry, transverse loading and material deformation: (Left) non-deformed configuration, (Right) deformed configuration.

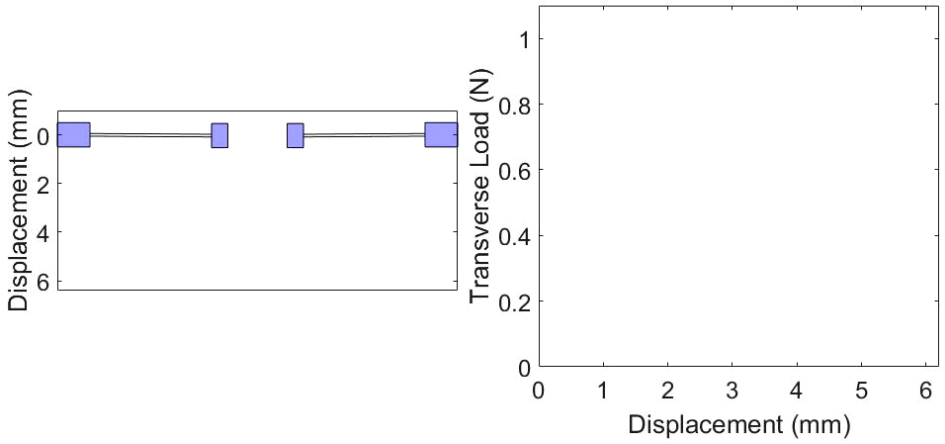

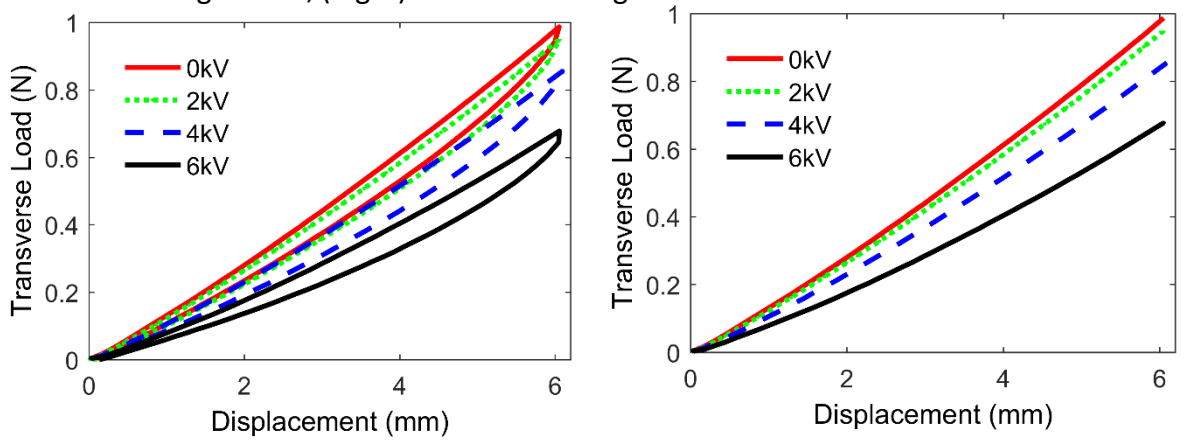

Figure: Transverse load data: (Left) Complete load/unload cycle and (Right) load cycle used for model calibration. Data collected by Adriane Moura and Wei Gao.

Theory: Transverse Force – Displacement

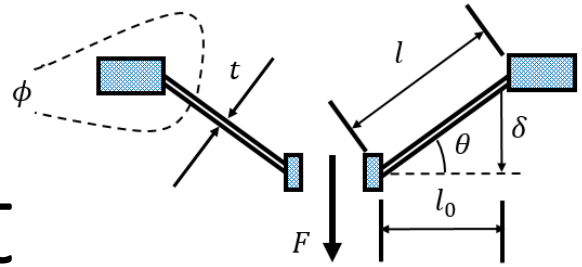

- Transverse load[1]

$$F = 2\pi \sin(\theta)\, rt\sigma_l$$

- Cauchy stress in radial direction. Application of electric field in transverse direction decreases the Cauchy stress[2],

$$\sigma_l = \sigma_l^H - \kappa_r \epsilon_0 E_t^2$$

where the relative permittivity, κ_r, is assumed independent of deformation.

- Non-affine hyperelastic stress assuming incompressibility[3].

$$\sigma_l^H = \frac{G_c}{3}\left(\lambda_{l,tot}^2 - \frac{1}{\lambda_{c,pre}^2 \lambda_{l,tot}^2}\right)\left(\frac{9\lambda_{max}^2 - I_1}{3\lambda_{max}^2 - I_1}\right) + G_e\left(\lambda_{l,tot}\left(1 + \lambda_{c,pre}\right) - \frac{1 + \lambda_{c,pre}}{\lambda_{c,pre}\lambda_{l,tot}}\right)$$

1. Rizzello, Gianluca, et al. "Dynamic Electromechanical Modeling of a Spring-Biased Dielectric Electroactive Polymer Actuator System." ASME 2014 Conference on Smart Materials, Adaptive Structures and Intelligent Systems. American Society of Mechanical Engineers, 2014.
2. Zhao, Xuanhe, Wei Hong, and Zhigang Suo. "Electromechanical hysteresis and coexistent states in dielectric elastomers." Physical review B 76.13 (2007): 134113.
3. Davidson, Jacob D., and N. C. Goulbourne. "A nonaffine network model for elastomers undergoing finite deformations." Journal of the Mechanics and Physics of Solids 61.8 (2013): 1784-1797.

Parameter Estimation: Transverse Force – Displacement

- $\theta = [G_c, G_e, \lambda_{max}]$
  - Calibrated at zero field cases

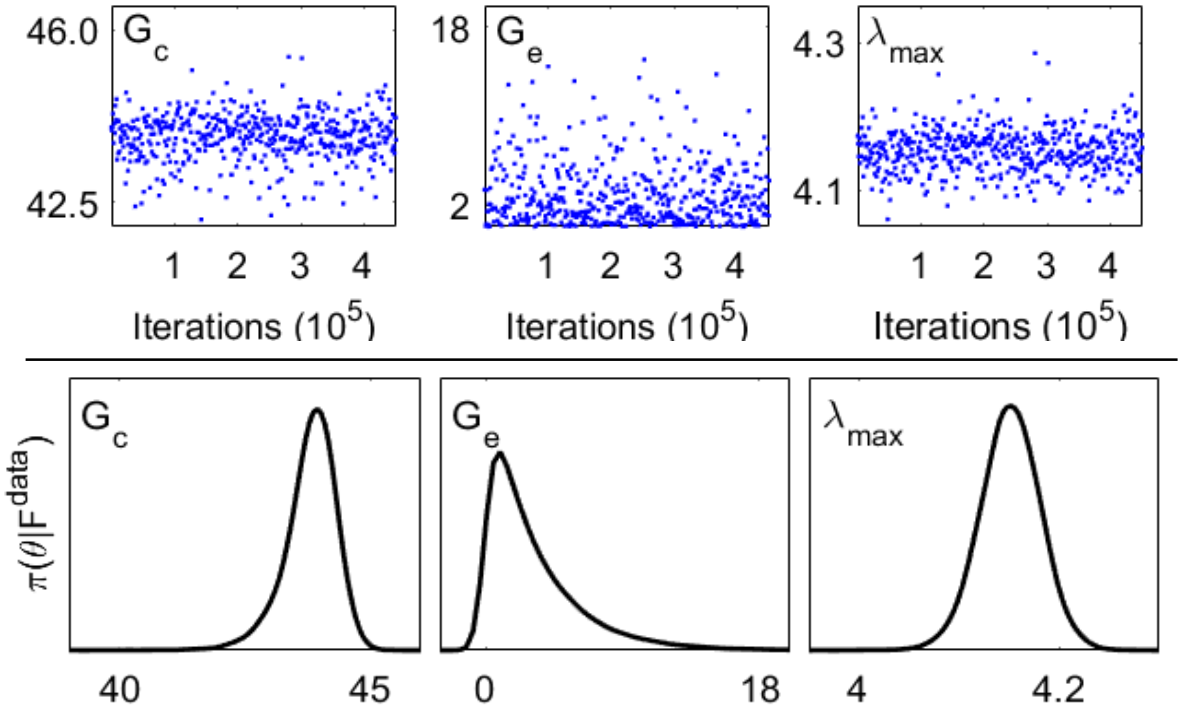

- $\theta = [\kappa_r]$
  - Calibrated at non-zero field cases

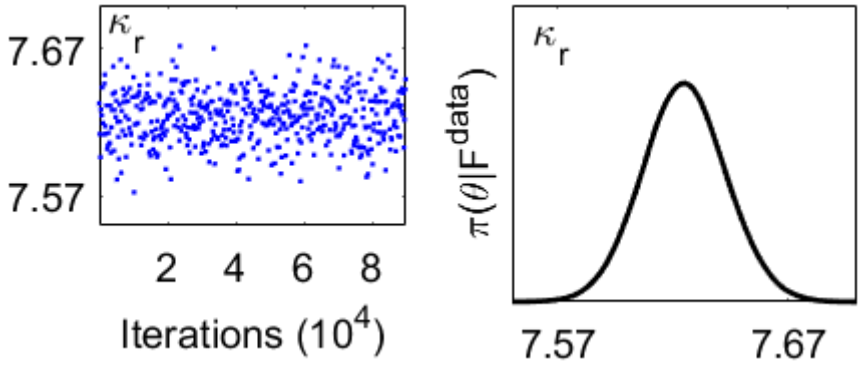

Uncertainty Propagation: Transverse Force – Displacement

- Calibration:
  - All data from four specimens
  - Each specimen tested from $0 - 6\ kV$
- Reasonable prediction at all voltage levels

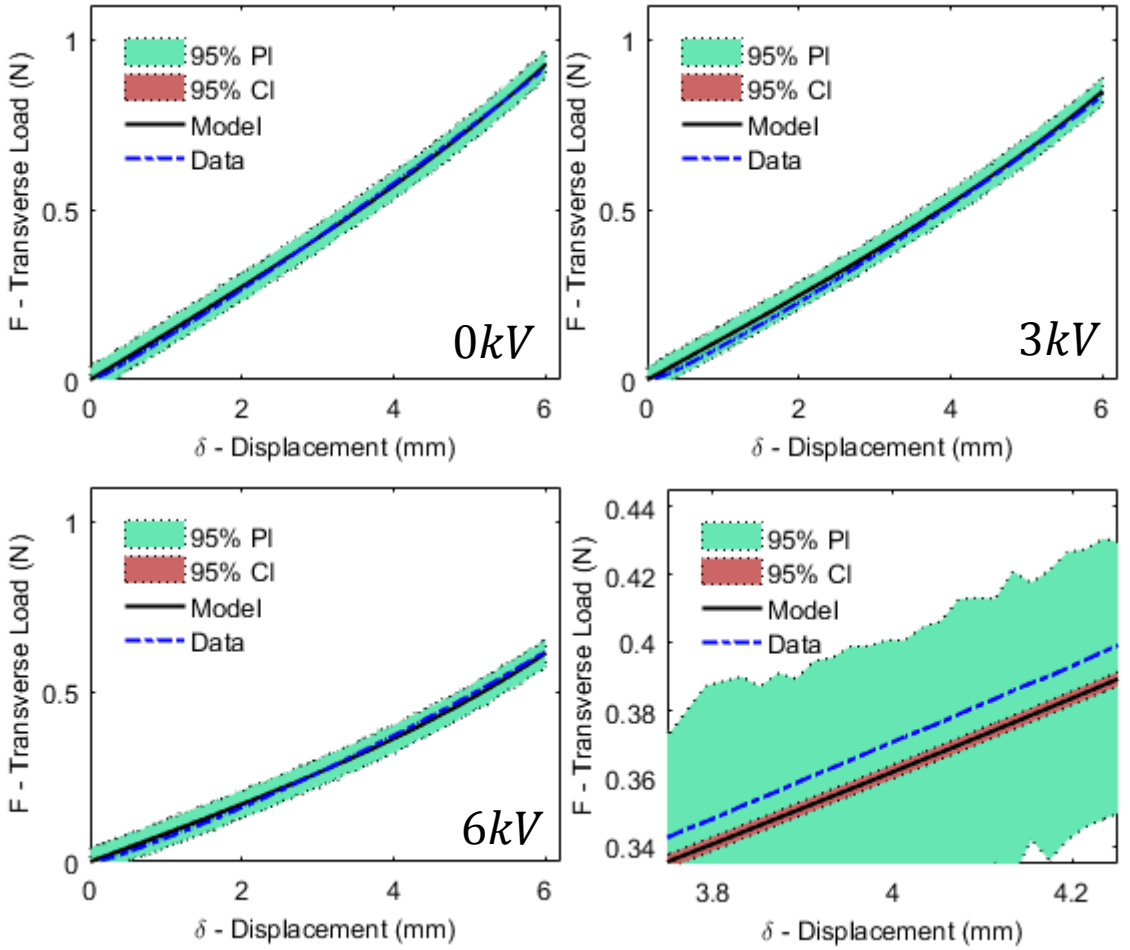

Experimental Setup: Electric Displacement – Electric Field

- Sawyer-Tower circuit
  - Applied sinusoidal voltage
    - Amplitudes ranging from $1 - 6\ kV$
  - VHB specimen placed in series with a known capacitor
- Considered capacitance in deformed and non-deformed configurations.

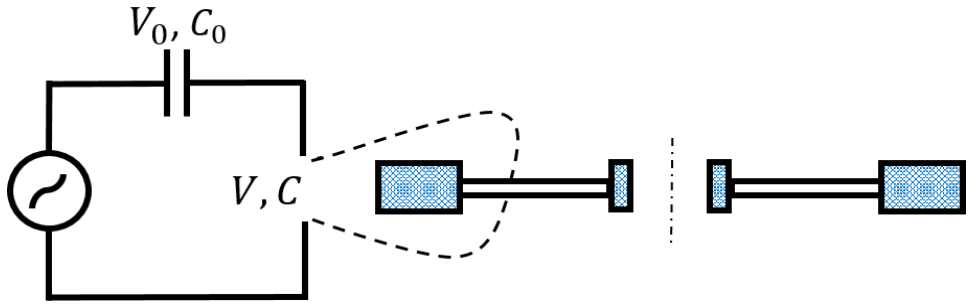

Figure: Sawyer-Tower circuit with VHB in series with 153 μF capacitor (C_0). VHB specimen measured from non-deformed configuration.

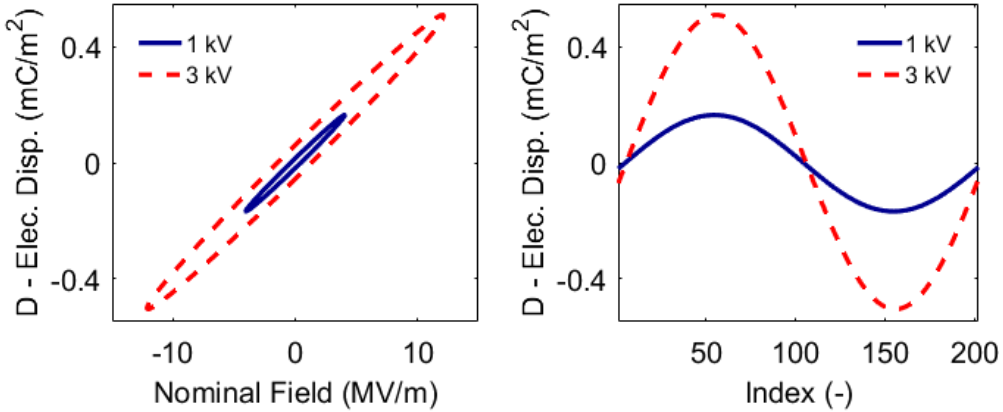

Figure: Data collected from Sawyer-Tower circuit: (Left) Electric displacement plotted as a function of the nominal field and (Right) electric displacement as a function of index from a single loop. Data collected by Wei Gao and Adriane Moura.

Experimental Observations: Electric Displacement – Electric Field

- Relative permittivity: slope of electric displacement versus electric field data

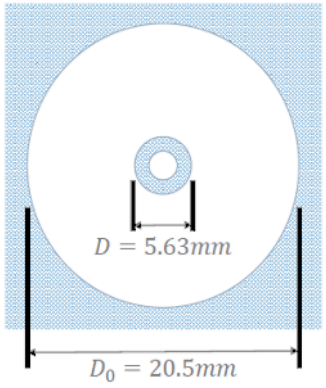

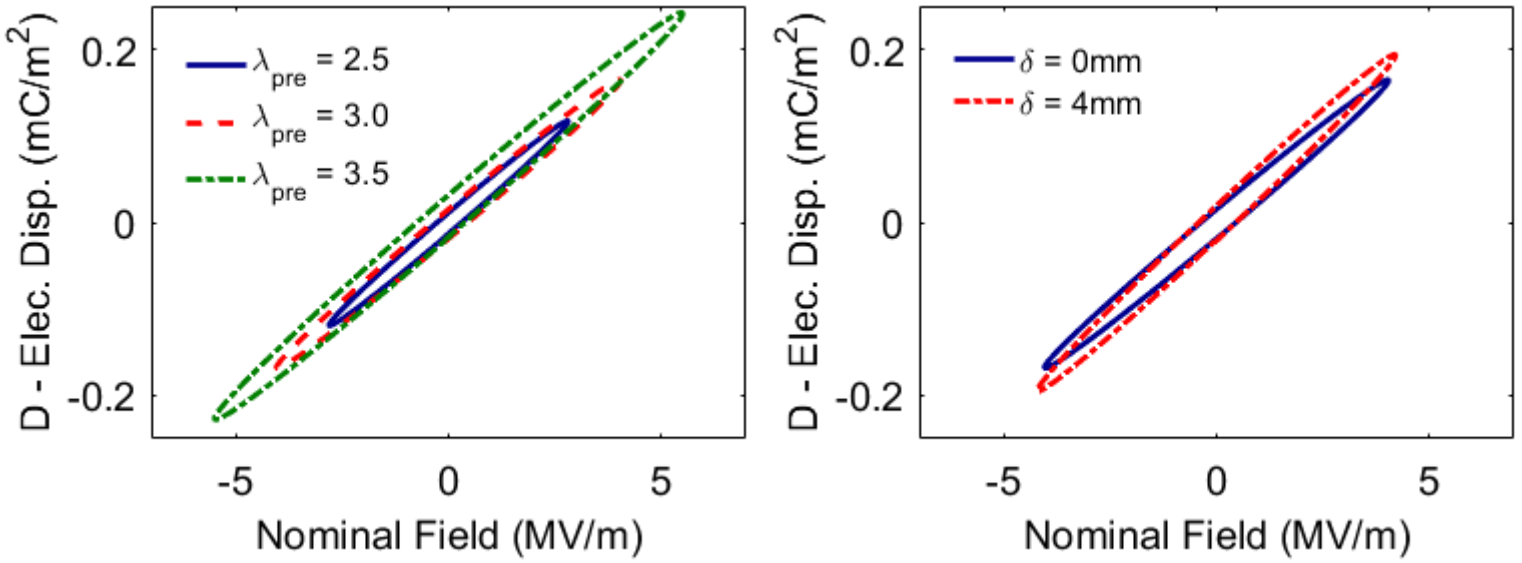

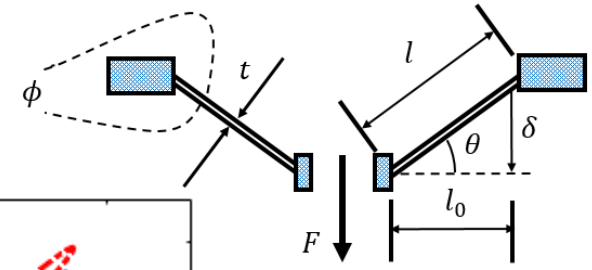

Figure: (Left) Negligible change in slope by changing the pre-stretch and (Right) clear slope change due to transversely displacing membrane - unclear what mechanism causes this change in permittivity.

Theory:
Electric Displacement – Electric Field

- Polarization model[1]

$$\ddot{P}_t + \gamma \dot{P}_t + \frac{K}{m} P_t = \frac{Ne^2}{m} E_t$$

- True electric displacement is related to the electric field by

$$D_t = \epsilon_0 E_t + P_t$$

Note the nominal and true electric field should be the same under the assumption that the membrane does not buckle.

- Ignoring 2nd order rate effects yields the rate-dependent dielectric constitutive model

$$\tau \dot{D}_t + D_t = \tau \epsilon_0 \dot{E}_t + \kappa_r \epsilon_0 E_t$$

where $\kappa_r \epsilon_0 = 1 + \frac{Ne^2}{K\epsilon_0}$ and $\tau = \frac{\gamma m}{K}$.

1. Fowles, Grant R. Introduction to Modern Optics. Courier Corporation, 2012.

Parameter Estimation: Electric Displacement – Electric Field

- $\theta = [\kappa_r, \tau_D]$

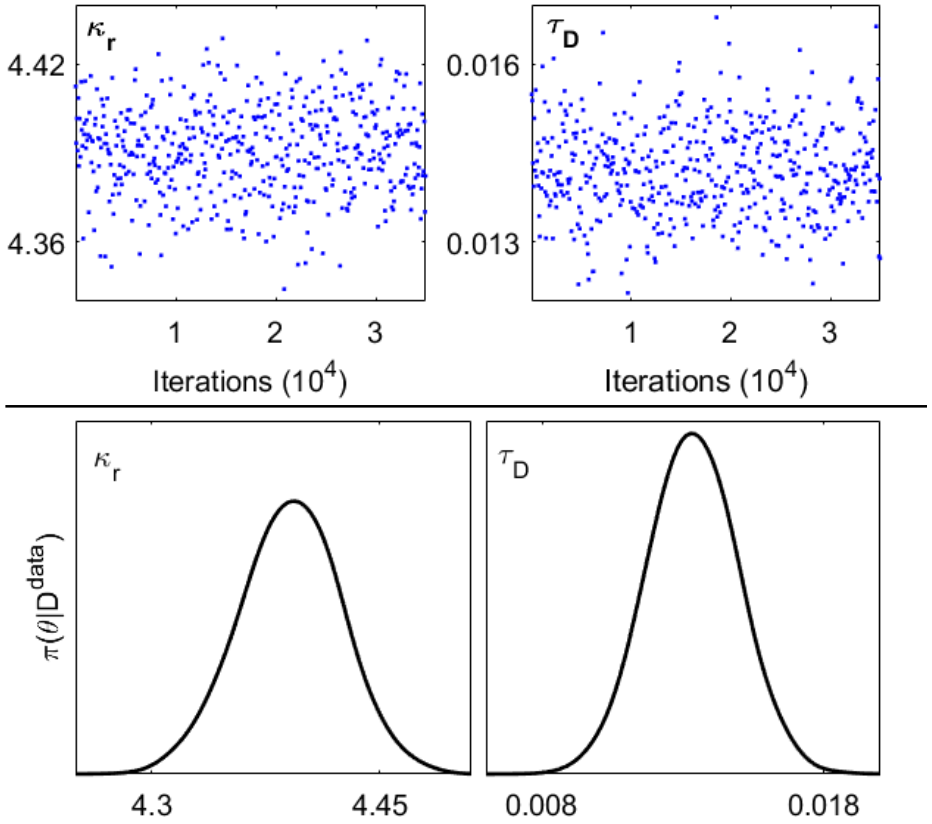

- Affect of pre-stretch and transverse displacement on κ_r

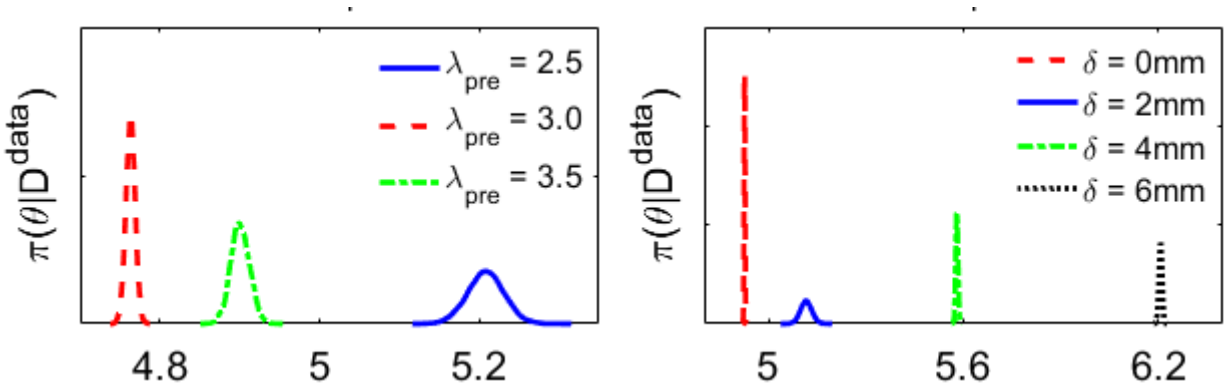

Uncertainty Propagation: Transverse Force-Displacement Model

- Calibration:
  - Four specimens
  - Amplitude of applied voltage: $2 - 5\ kV$
- Reasonable prediction at all voltage levels

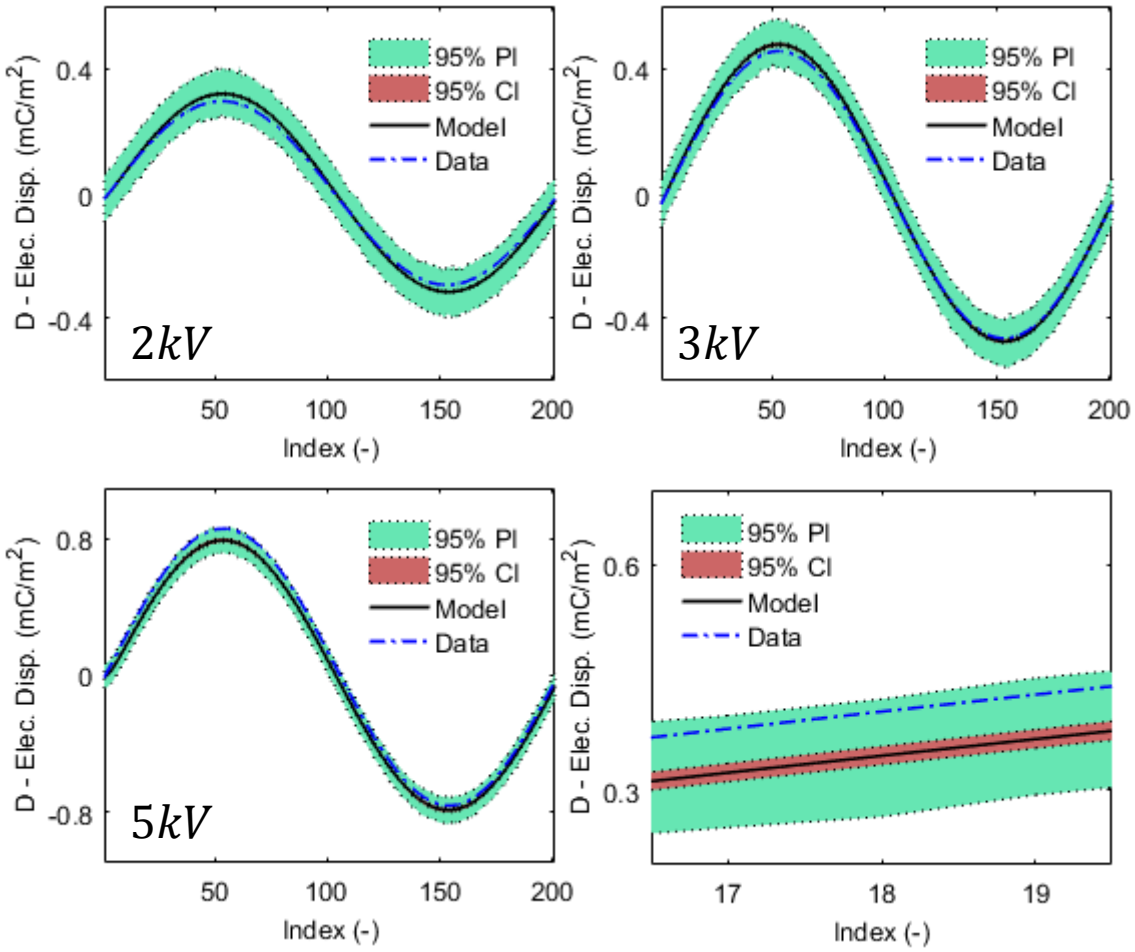

Transverse Force – Displacement
Electric Displacement – Electric Field

- Posterior densities:

$$\pi\left(\kappa_r \middle| M^{data}\right)$$

- Two sources:
  - Transverse Force – Displacement (TD)
  - Electric Displacement – Electric Field (DE)
- Conflict
  - Literature supports result found from DE experiment

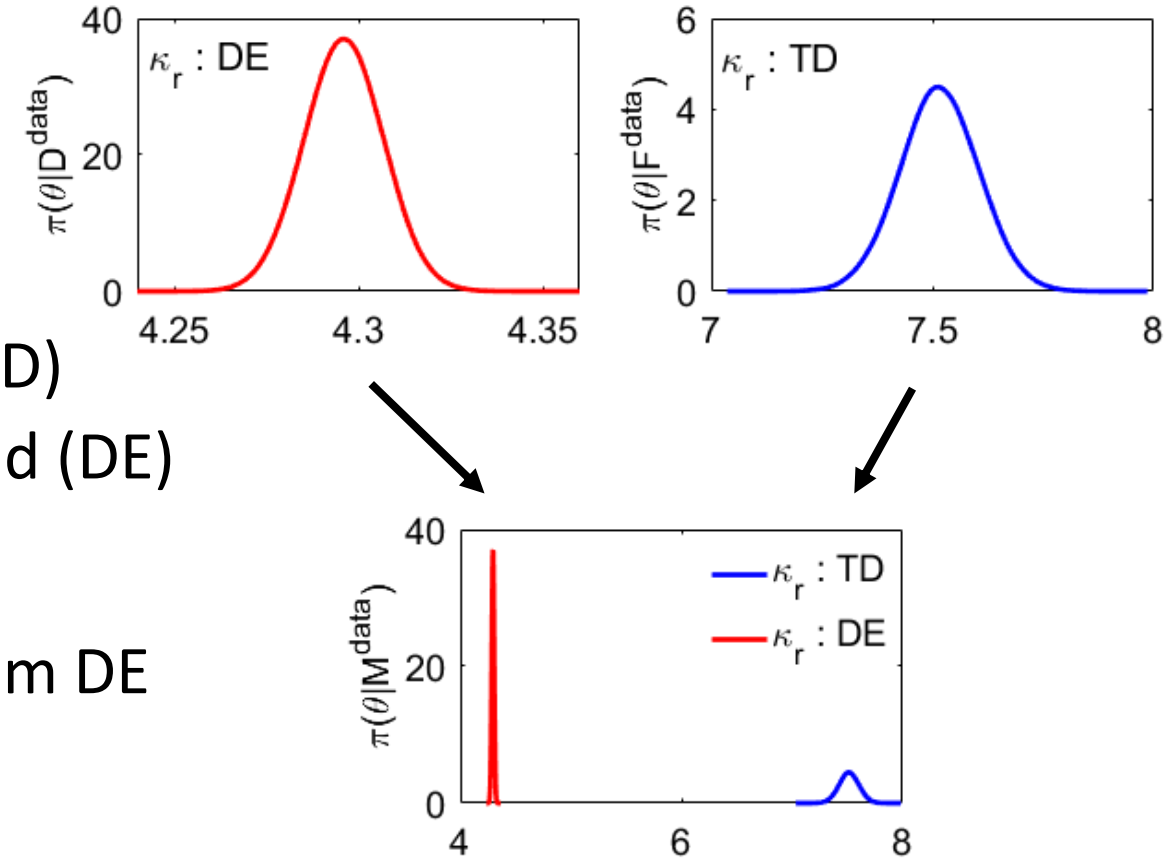

Conclusions & Future Work: Electrostriction

- Conclusions:
  - Experimentally characterized loading of pre-stretched membranes under different electrostatic fields
  - Analyzed uncertainty in how we model relative permittivity
- Questions:
  - Is there deformation dependent permittivity?
  - Is the assumed deformation profile a reasonable approximation?

Publications: Electrostriction

Publications:

- Miles, P., Guettler, A., Hussaini, M. Y., Oates, W. "**Uncertainty Analysis of a Dielectric Elastomer Membranes Under Multi-Axial Loading**." *ASME Smart Materials, Adaptive Structures, and Intelligent Systems*, 2015. Best Student Paper Award in Mechanics & Behavior of Active Materials.

Pending Publications:

- Miles, Paul, Gao, W., Moura, A., Hussaini, M.Y., Oates, W. "**Uncertainty Analysis of Dielectric Elastomer Membranes Under Electromechanical Loading**."

Ferroelectrics: Quantum-Informed Continuum Modeling

Materials: Ferroelectrics

- Applications:
  - Energy harvesting
  - Structural health monitoring
  - Flow control
  - Ultrasound
  - Robotics
  - Sonar
  - Nanopositioning

Figure: Piezoelectric ceramics are mechanically deformed when in the presence of an electric field. The reverse mechanism is also true, in that an electrical response is generated if a mechanical load is applied.

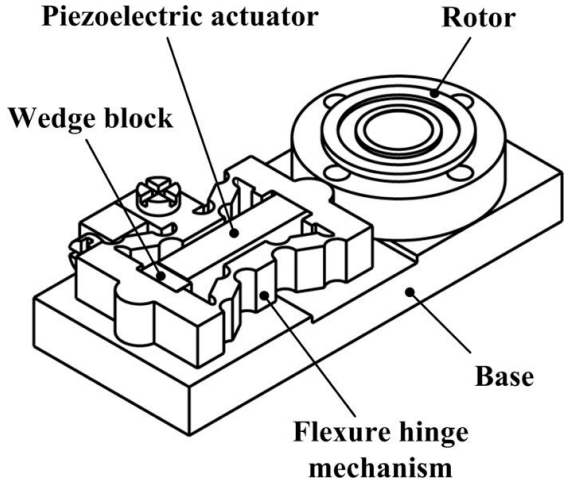

Figure: Schematic of nanoposition stage[1].

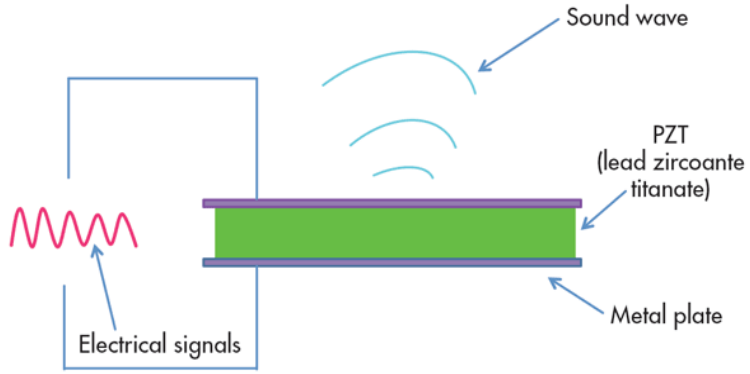

Figure: Schematic of piezoelectric in sonar transducer[2].

1. Li, Jianping, et al. "Design and experimental tests of a dual-servo piezoelectric nanopositioning stage for rotary motion." *Review of Scientific Instruments* 86.4 (2015): 045002.
2. http://www.electronicdesign.com/power/what-piezoelectric-effect

Ferroelectrics: Outline

- High Fidelity Simulations
  - Density Functional Theory (DFT)
- Theory: Continuum Model
  - Monodomain and Polydomain Structures
- Uncertainty Quantification
- Conclusions and Future Work

Ferroelectrics: Density Functional Theory (DFT)

- Lead Titanate: $PbTiO_3$
- Different atomic positions lead to different polarization states
- Uncertainty:
  - Nuclei positions and electron density (5 atoms, each with 3 degrees of freedom)
  - Approximate as a polarization vector

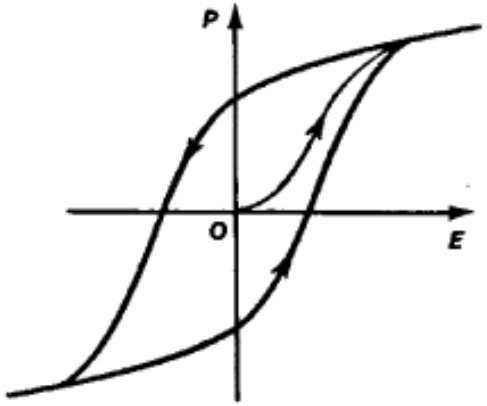

Figure: Polarization versus electric field measurements for ferroelectric material[1].

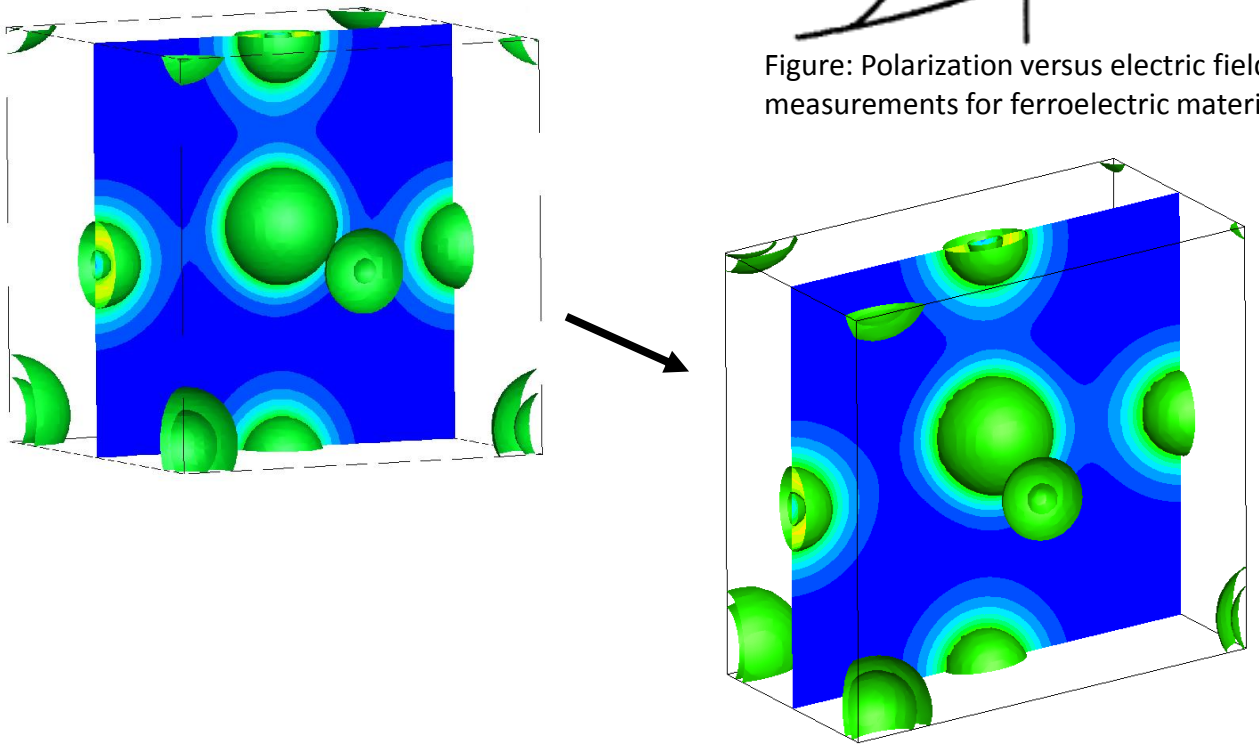

Figure: Example of the electron density solutions: (Left) Reference undeformed cubic structure and (Right) shear deformed state where the unit cell has been sheared such that the deformation gradient component F_{23} is non-zero.

1. http://encyclopedia2.thefreedictionary.com/Hysteresis+(electric)

Ferroelectrics: Density Functional Theory (DFT)

- Polarization states:
  - Atoms moved based on estimates from shear deformation
  - Positive P_2 generated, P_3 reduced
  - Polarization uniform in entire domain
- Calculate energy and stress at each polarization state

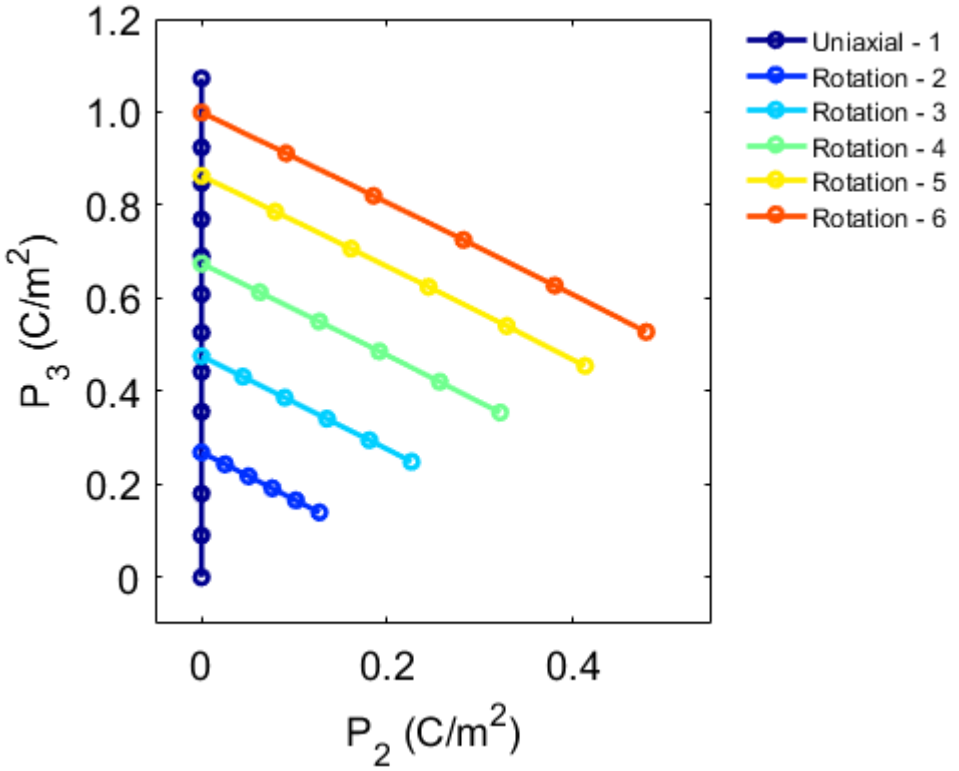

Figure: Polarization rotation – starting from five different locations of nonzero P_3 and $P_2 = 0$. Atoms moved along directions estimated from shear deformation states to generate positive P_2 values while reducing P_3. DFT computations performed by Justin Collins.

Theory: Continuum Model

- Free energy density

$$u(P_i, P_{i,j}, \Delta\varepsilon_{ij}) = u_M(\Delta\varepsilon_{ij}) + u_L(P_i) + u_C(P_i, \Delta\varepsilon_{ij}) + u_G(P_{i,j})$$

- Components
  - u_M - elastic energy
  - u_L - Landau energy
  - u_C - electrostrictive energy
  - u_G - polarization gradient energy
  - P_i - polarization in i^{th} direction
  - $P_{i,j}$ - polarization gradient
  - $\Delta\varepsilon_{ij}$ - strain

Theory: Continuum Model

- Landau energy density

$$u_L(P_i) = \alpha_1(P_1^2 + P_2^2 + P_3^2) + \alpha_{11}(P_1^2 + P_2^2 + P_3^2)^2$$
$$+ \alpha_{12}(P_1^2P_2^2 + P_2^2P_3^2 + P_1^2P_3^2) + \alpha_{111}(P_1^6 + P_2^6 + P_3^6)$$
$$+ \alpha_{112}[P_1^4(P_2^2 + P_3^2) + P_2^4(P_1^2 + P_3^2) + P_3^4(P_1^2 + P_2^2)]$$
$$+ \alpha_{123}P_1^2P_2^2P_3^2$$

- Unknown phenomenological parameters: $\alpha_1, \alpha_{11}, \dots, \alpha_{123}$

Uncertainty Quantification: Monodomain Structures

- Posterior densities: $\pi(\theta|M^{data})$

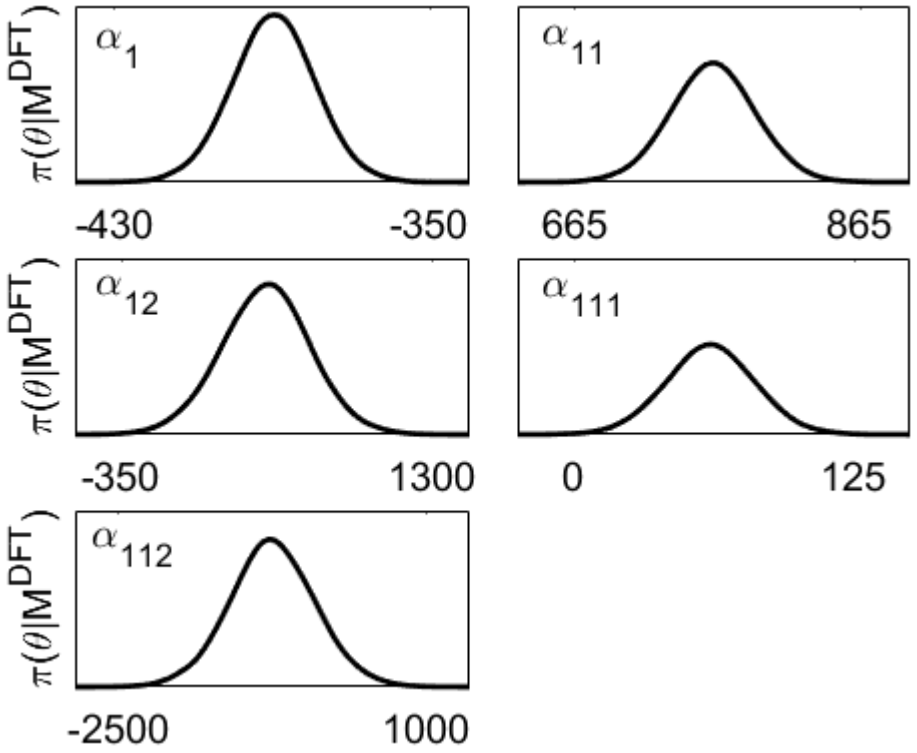

- Pairwise correlation:

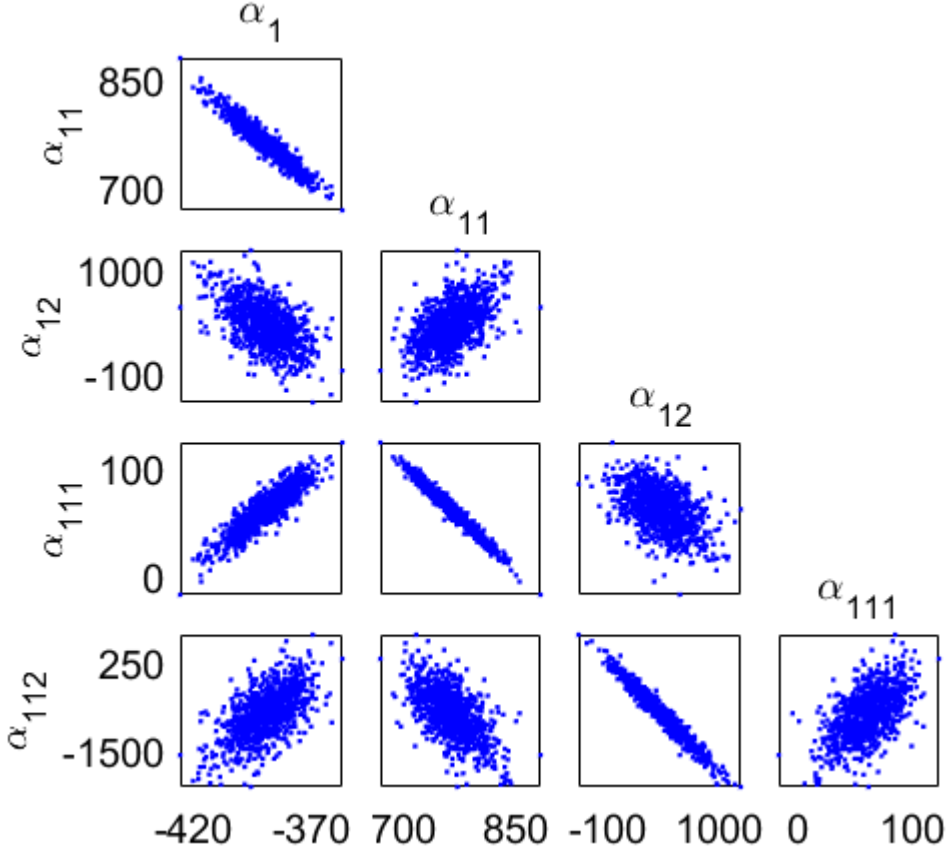

Uncertainty Propagation: Monodomain Structures

- Energy density: u
- Stress: σ_{11}

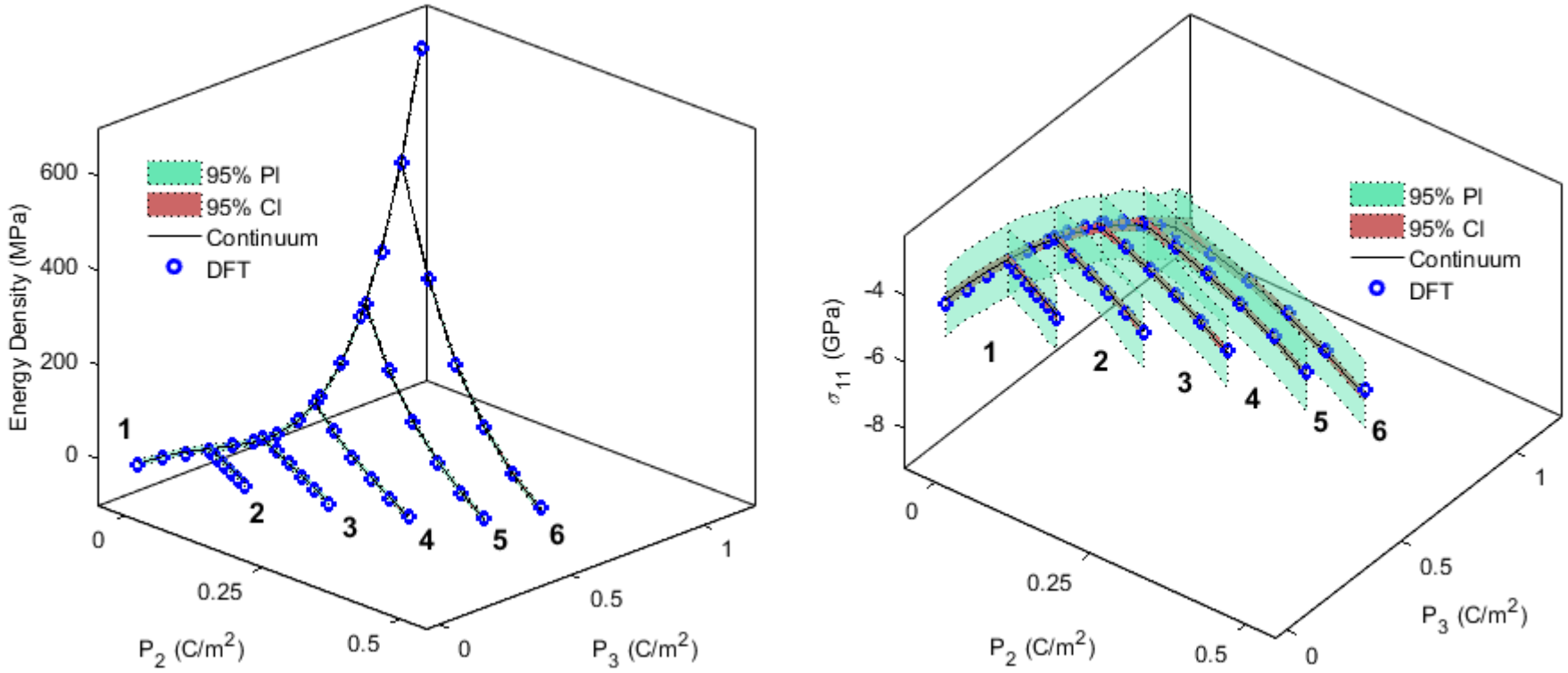

Figure: (Left) Uncertainty propagation through energy model and (Right) uncertainty in normal stress in the x_1 direction.

Polydomain Structures

- Atomic structure broken up into domains
  - Domains – regions of uniform polarization
- Domains divided by walls
  - Most active material behavior occurs along domain wall
  - Extending work done by Cao & Cross[1] and Meyer & Vanderbilt[2].

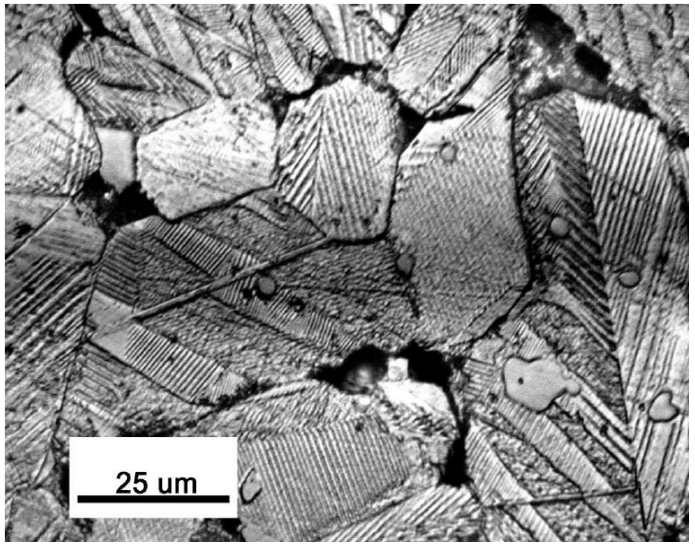

Figure: Domain structures in Barium Titanate[3].

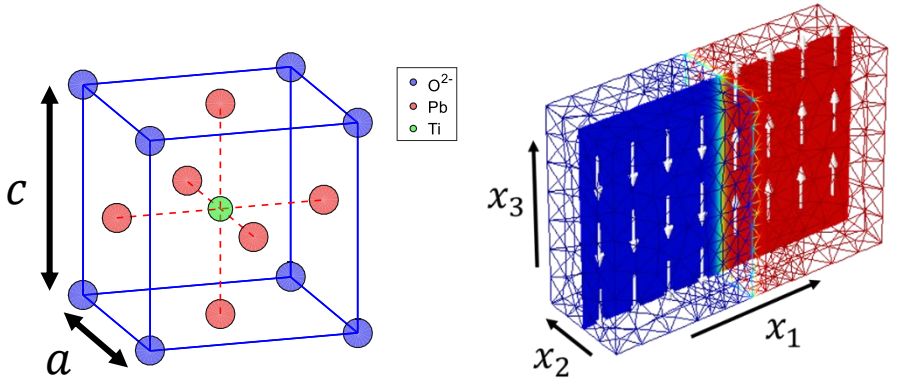

Figure: (Left) Unit cell width is approximately 4 angstroms. (Right) Domains separated by walls that are approximately 5 angstroms wide.

1. Cao, W., and Cross, L.E. "Theory of Tetragonal Twin Structures in Ferroelectric Perovskites with a First-Order Phase Transition." *Physical Review B* 44.1 (1991)
2. Meyer, B., and Vanderbilt, D. "*Ab initio* study of ferroelectric domain walls in $PbTiO_3$". Physical Review B, 65(10):104111, 2002.
3. Liang, D., Stone, D., and Lakes, R. "Softening of bulk modulus and negative Poisson ratio in barium titanate ceramic near the Curie point." *Philosophical Magazine Letters* 90.1 (2010): 23-33.

Polydomain Structures

- 180° Domain Wall

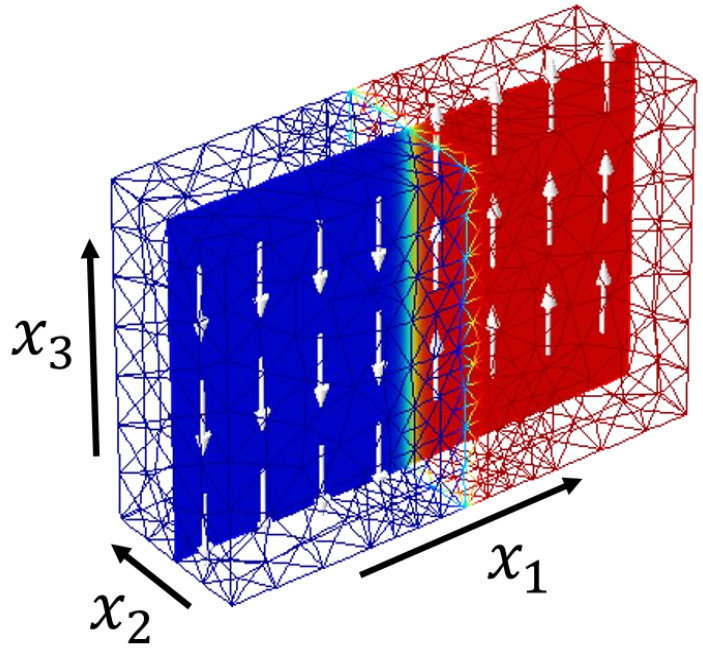

Figure: $180°$ domain wall – two distinct polarization regions. On the left (blue) we have polarization in the negative x_3 direction and on the right (red) the polarization is in the positive x_3 direction. The polarization switches by 180^o as you pass through the domain wall.

- 90° Domain Wall

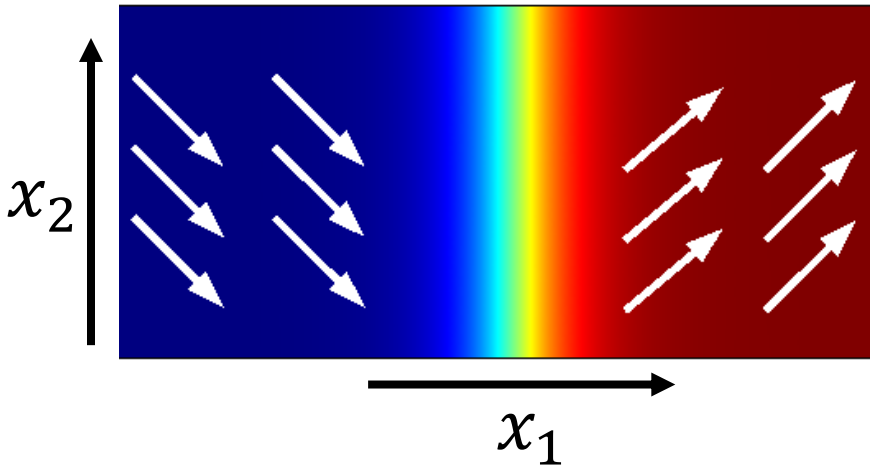

Figure: $90°$ domain wall – two distinct polarization regions. On the left (blue) we have polarization with components in the positive x_1-direction and negative x_2-direction. On the right (red) the polarization is in the positive x_1- and x_2-direction. The polarization switches by 90^o as you pass through the domain wall.

Polydomain Structures: 180° Domain Wall

- Energy associated with domain wall:

$$u - u_0$$

- Verified numerical solution using finite difference (FD) and finite element (FEA) formulation

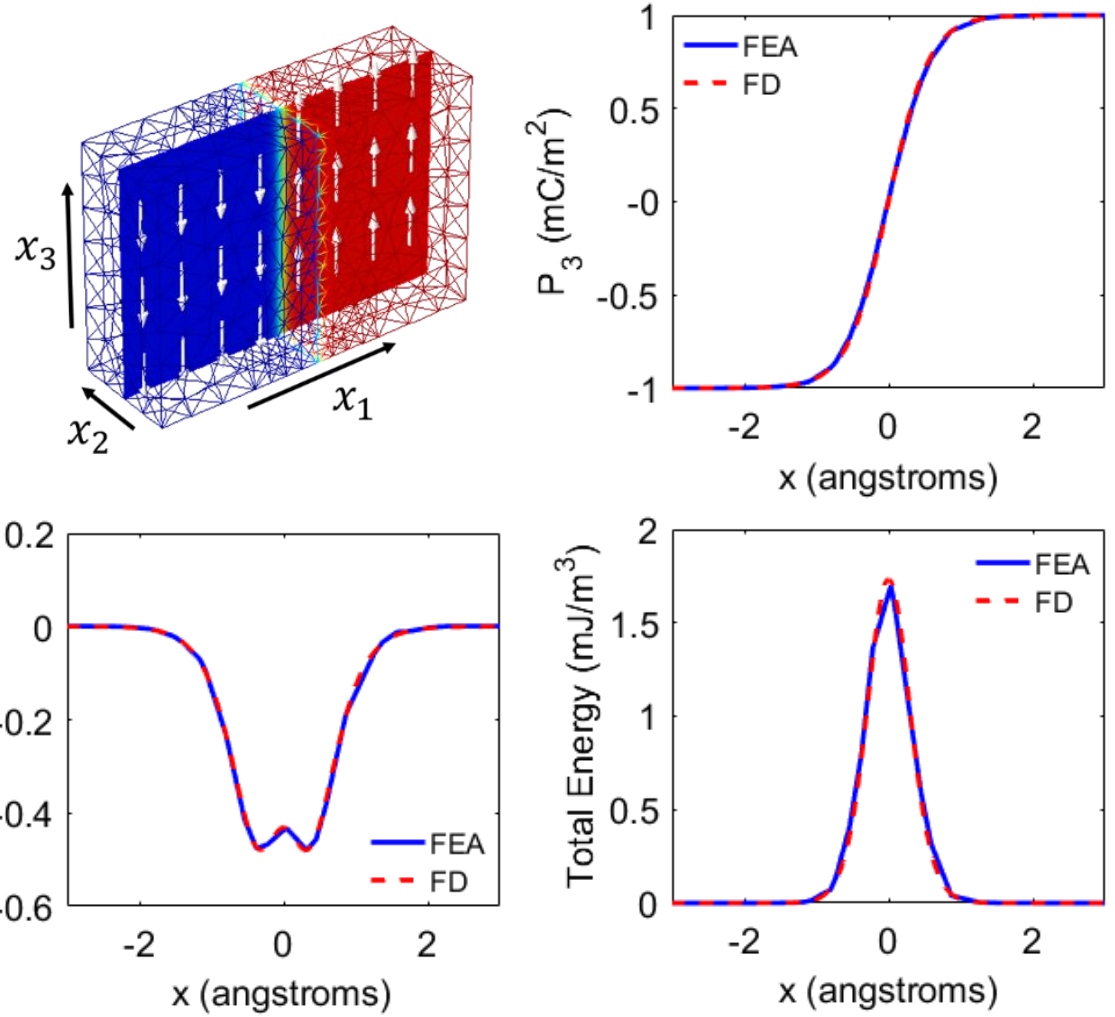

Figure: 180° domain wall energy along x_1-axis. (Top Right) Polarization switches from negative to positive within the nanoscale domain wall region. Compared solution found using FEA and FD: (Bottom Left) Landau energy density and (Bottom Right) total energy density.

Polydomain Structures: 180° Domain Wall

- Domain wall energy

$$E_{180^\circ} = \int_{-\infty}^{\infty} (u - u_0) dx_1$$

- From literature[1]: $E_{180^\circ} = 132$ mJ/m²

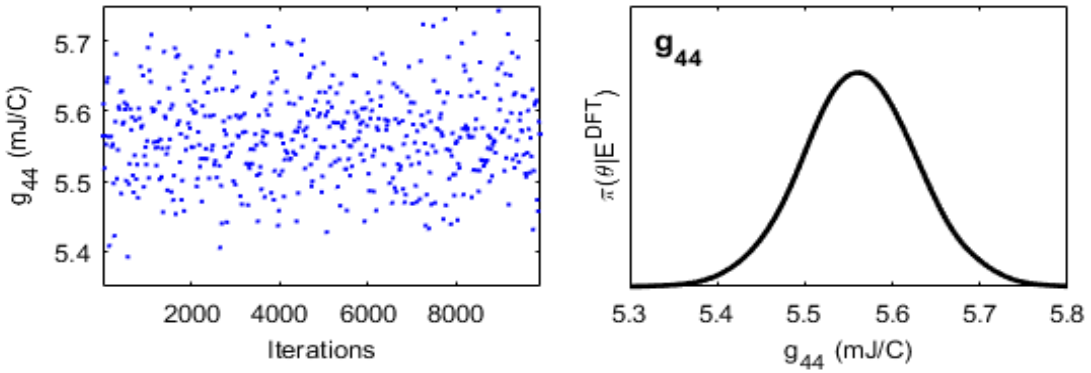

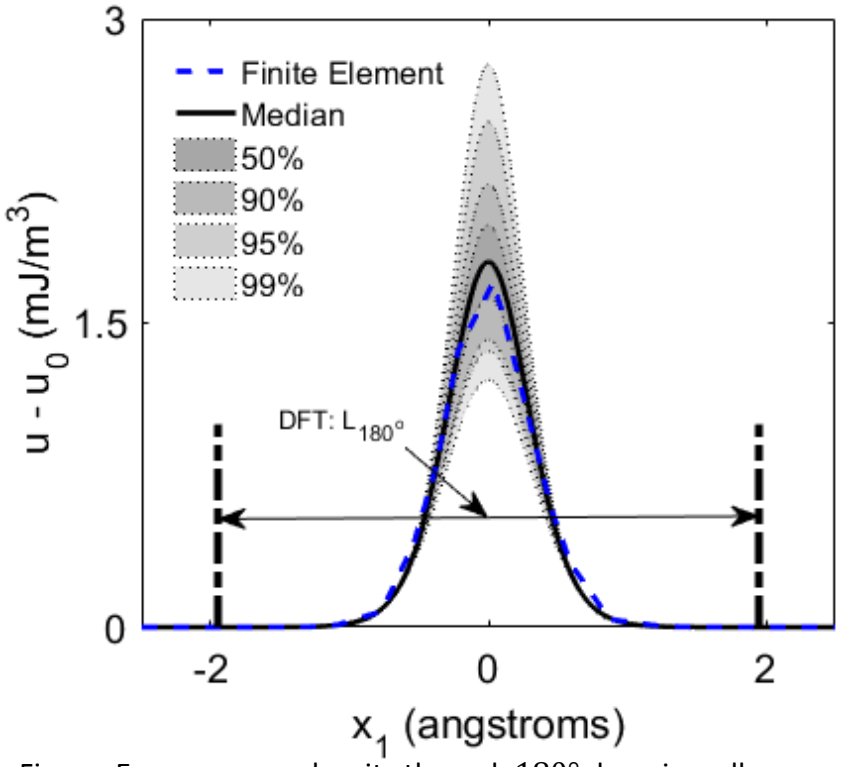

Figure: Excess energy density through 180° domain wall energy along x_1-axis. Uncertainty from continuum model parameters propagated through to generate 50% - 99% credible intervals.

1. Meyer, B., and Vanderbilt, D. "*Ab initio* study of ferroelectric domain walls in $PbTiO_3$". Physical Review B, 65(10):104111, 2002.

Conclusions & Future Work: Quantum Informed Continuum Modeling

- Conclusions:
  - Quantified model parameter uncertainty in monodomain structures
  - Developed numerical approximations for $180°$ and $90°$ domain wall structures
- Questions:
  - Is there parameter correlation between monodomain and polydomain structure parameters[1]?

1. Collaborative effort with Dr. Ralph Smith and Lider Leon at North Carolina State University.

Publications:
Quantum Informed Continuum Modeling

Publications:

- Miles, P., Leon, L., Smith, R., Oates, W. "**Uncertainty Analysis of Continuum Phase Field Modeling in 180 Degree Domain Wall Structures**." *SPIE Smart Structures and Materials + Nondestructive Evaluation and Health Monitoring*, 2017.
- Leon, L., Smith, R., Miles, P., Oates, W. "**Global Sensitivity Analysis for a Quantum Informed Ferroelectric Phase Field Model.**" *SPIE Smart Structures and Materials + Nondestructive Evaluation and Health Monitoring*, 2017.
- Leon, L., Smith, R., Oates, W., Miles, P. "**Sensitivity Analysis of a Quantum Informed Ferroelectric Energy Model**." *ASME Smart Materials, Adaptive Structures, and Intelligent Systems*, 2016.
- Oates, W., Miles, P., Leon, L., Smith, R. "**Uncertainty Analysis of Continuum Scale Ferroelectric Energy Landscapes Using Density Functional Theory**." *SPIE Smart Structures and Materials + Nondestructive Evaluation and Health Monitoring*, 2016.

Pending Publications:

- Miles, P., Leon, L., Smith, R., Oates, W. "**Analysis of a Multi-axial Quantum-Informed Ferroelectric Continuum Model: Part I Uncertainty Quantification**." 2017, in preparation.
- Leon, L., Smith, R., Oates, W., Miles, P. "**Analysis of a Multi-axial Quantum-Informed Ferroelectric Continuum Model: Part II Sensitivity Analysis**." 2017, in preparation.
- Miles, P., Leon, L., Smith, R., Oates, W. "**Uncertainty Analysis of Ferroelectric Polydomain Structures**." *ASME Smart Materials, Adaptive Structures, and Intelligent Systems*, 2017, accepted.
- Leon, L., Smith, R., Oates, W., Miles, P. "**Identifiability and Active Subspace Analysis for a Polydomain Ferroelectric Phase Field Model**." *ASME Smart Materials, Adaptive Structures, and Intelligent Systems*, 2017, accepted.

Acknowledgements

Committee:

- Dr. William Oates
- Dr. M. Yousuff Hussaini
- Dr. Changchun Zeng
- Dr. Kunihiko Taira
- Dr. Shangchao Lin
- Dr. Ralph Smith

Experimental Research:

- Wei Gao, Adriane Moura, Justin Collins, and Dr. Michael Hays

Fractional order methods:

- Dr. Somayeh Mashayekhi

Lab Colleagues:

- Dr. Oates's Research Group
- Dr. Taira's Research Group

Support:

- P.M. gratefully acknowledges support from the Army Research Office through grant W911NF-13-1-0146, program manager Matt Munson. This work has also been supported by NSF CDS&E awards (CMMI grants 1306320 and 1306290).
- Additional support provided by Florida State University's *Legacy Fellowship.*
- National Science Foundation (NSF) Research Experience for Undergraduates (REU)
  - Multi-physics of Active Systems and Structures (MASS)